2016

Quantifying the spatial distribution of intradiscal pressure and its assessment via non-invasive estimates of intervertebral disc degeneration

BOSTON UNIVERSITY

COLLEGE OF ENGINEERING

Thesis

QUANTIFYING THE SPATIAL DISTRIBUTION OF INTRADISCAL PRESSURE AND ITS ASSESSMENT VIA NON-INVASIVE ESTIMATES OF INTERVERTEBRAL DISC DEGENERATION

by

ALEXANDER M. DELMONACO

B.S., Boston University, 2014

Submitted in partial fulfillment of the

requirements for the degree of

Master of Science

2016

Approved by

First Reader

Elise F. Morgan, Ph.D.
Professor of Biomedical Engineering
Professor of Mechanical Engineering

Second Reader

Paul E. Barbone, Ph.D.
Professor of Mechanical Engineering

Third Reader

Katherine Yanhang Zhang, Ph.D.
Associate Professor of Mechanical Engineering
Associate Professor of Biomedical Engineering

To Mom, Dad, Nick and Kerie

ACKNOWLEDGEMENTS

Thank you to Alexander Adams, Dr. Glenn Barest, Andy Camp, Cameron Curtiss, Jesse Connell, Joe Estano, Paul Fein, Amira Hussein, Timothy Jackman, Ryan Lacy, Kamil Makhnejia, Dr. Elise Morgan, Bob Sjostrom, and Zack Webster for your substantial contributions to this work.

QUANTIFYING THE SPATIAL DISTRIBUTION OF INTRADISCAL PRESSURE AND ITS ASSESSMENT VIA NON-INVASIVE ESTIMATES OF INTERVERTEBRAL DISC DEGENERATION

ALEXANDER M. DELMONACO

ABSTRACT

Intervertebral disc (IVD) degeneration is strongly associated with back pain, and affects approximately 60% of the population by age 70. Furthermore, it has been suggested that this degeneration may play an important role in the initiation or perpetuation of vertebral fractures. Given that the IVD is a primary load-bearing structure in the spine, the change of intradiscal pressure (IDP) over time that accompanies disc degeneration provides a functional measure of the disease pathology. Studies show that both an overall decrease in IDP magnitude and changes in the spatial distribution of IDP are found with increasing levels of degeneration. Thus, the overall goal of this study was to determine the correlation between the spatial distributions of IDP, as measured along both mid-sagittal and mid-coronal paths, and a clinically feasible assessment of disc health. Disc degeneration was assessed non-invasively using quantitative computed tomography (QCT). A custom, electro-mechanical device was designed, manufactured and assembled to measure IDP distributions. The results indicated that the spatial distribution of IDP was most homogenous for the nucleus pulposus (NP) region regardless of load type and disc health grade. Mean IDP tended to be lowest in severely degenerated discs, consistent with earlier findings that axial loads in spinal columns with degenerated IVDs shift from the disc to the neural arch in both flexural and erect postures.

TABLE OF CONTENTS

LIST OF TABLES

LIST OF FIGURES

LIST OF ABBREVIATIONS

AF ..... Annulus Fibrosus

ALDI ..... Apparent Loss of Disc Integrity

ANOVA ..... Analysis of Variance

FE ..... Finite Element

GAG ..... Glycosaminoglycan

IVD ..... Intervertebral Disc

MRI ..... Magnetic Resonance Imaging

NP ..... Nucleus Pulposus

PBS ..... Phosphate Buffer Saline (Solution)

PDMS ..... Polydimethylsiloxane

PMMA ..... Polymethyl Methacrylate

QCT ..... Quantitative Computed Tomography

CHAPTER ONE

MOTIVATION

Vertebral fractures affect 12–20% of men and women over the age of 50.[1] In addition, cumulative mortality rates following vertebral fractures are larger than other osteoporotic sites including the hip, shoulder, and forearm.[2] Although the prevalence of vertebral fracture is particularly high, how these fractures occur is not fully understood. It has been suggested that degeneration of adjacent intervertebral discs (IVDs) with age may affect the risk of vertebral fracture.[3–6] The IVD is a primary load-bearing structure in the spine. Physiological and chemical changes to the IVD associated with aging are primary causes of disc degeneration,[7] as conformational changes such as disc-space narrowing (DSN) cause depressurization of the IVD and further perturb intradiscal mechanics.[8] Degeneration of the IVD affects a large portion of the population: 10% of 50-year-old and 60% of 70-year-old IVDs show severe degeneration, and men are more often affected than women.[9] Moreover, IVD degeneration has been strongly associated with self-reported back pain among the aging population.[10]

Measurements of intradiscal pressure (IDP)[11–14] associated with disc degeneration allow for a quantitative assessment of disease pathology. Changes in the distribution of pressure within the IVD may place the vertebral endplate at risk for fracture.[15–19] Such changes as well as a loss of IDP overall have been found to correlate with increasing levels of IVD degeneration.[20]

Few studies have examined whether non-invasive methodologies of assessing IVD degeneration correlate with degenerative changes in IDP. Previous work in establishing a quantitative computed tomography (QCT) –based grading scale for disc

degeneration has been carried out, and is characterized by the "apparent loss of disc integrity" (ALDI) grade.[21] The overall goal of this study was to determine the correlation between the spatial distributions of IDP measured along mid-sagittal and mid-coronal paths, and a clinically feasible, non-invasive assessment of disc health, the ALDI grade

INTRODUCTION

Vertebral Anatomy

The spine is a primary unit of structure and function in the body, and is comprised of two major components: the vertebra and the intervertebral disc. The vertebra functions to bear loads and to protect the spinal cord. The vertebra is comprised of a vertebral body and posterior elements (Figure 1.1). Each vertebral body is comprised of trabecular bone surrounded by a thin shell of cortical bone. The posterior elements are comprised mostly of cortical bone.

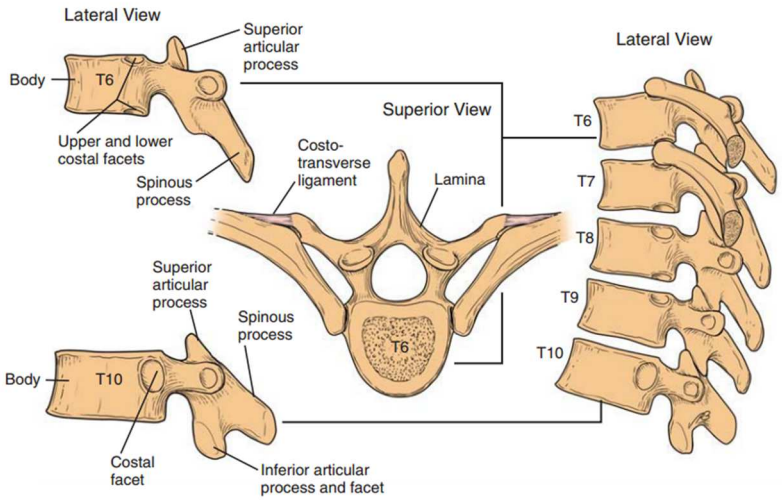

Figure 1.1 Schematic of various human thoracic vertebrae. Lateral views of T6 (top left) and T10 (bottom left) vertebrae, superior view of T6 vertebra (center), and lateral view of T6–T10 vertebrae.[22]

Intervertebral Disc Anatomy

Intervertebral discs (IVDs) are interstitial, fibrocartilaginous components of the spine. The IVD functions to transmit loads between adjacent vertebrae, while also offering flexibility to the spinal column[23] (Figure 1.2A). IVDs are comprised of a centrally located, gelatinous tissue known as the nucleus pulposus (NP), surrounded by a layered, fibrocartilaginous structure known as the annulus fibrosus (AF) (Figure 1.2B). The healthy NP has a high water content, due in part to its high concentration of negatively charged proteoglycans, which create an osmotic pressure gradient that draws water into the NP.[24,25] Hydrostatic pressure from compressive loads is transmitted radially from the NP to the surrounding AF.[26]

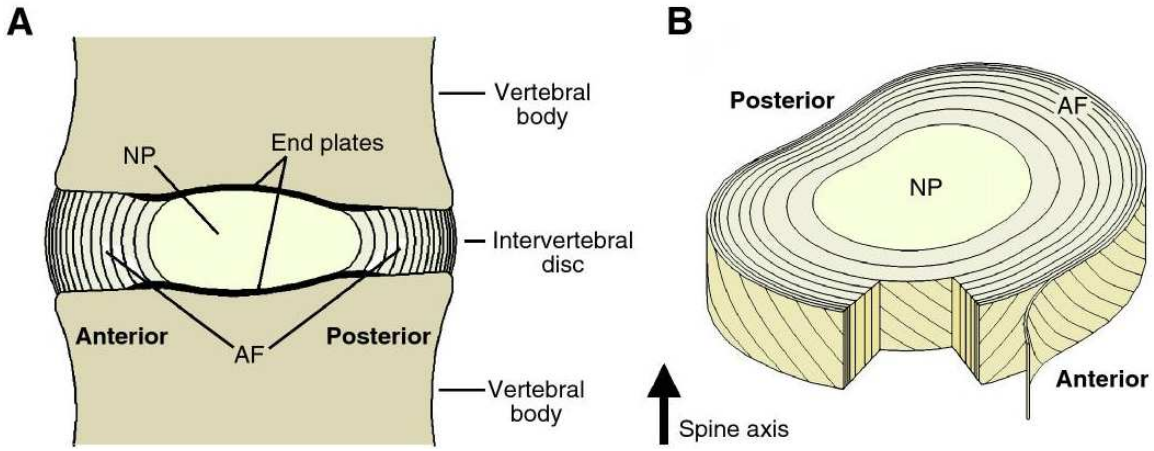

Figure 1.2 (A) Mid-sagittal cross section of intervertebral disc and surrounding vertebral bodies. (B) Isometric view of intervertebral disc showcasing nucleus pulposus (NP) and annulus fibrosus (AF) lamellar orientation.[27]

Intervertebral Disc Degeneration and Diagnostic Techniques

Degeneration in the IVD has been strongly associated with back pain.[10] Additionally, the progression of this degeneration is linked with an increase in age[28];

approximately 10% of 50-year-old IVDs, and 60% of 70-year-old IVDs show severe degeneration.[9] With increasing age, the proteoglycan content of the NP tends to decrease, which leads to loss of hydration and hydrostatic swelling pressure.[23,25] A marked decrease in IDP across the NP has been identified in degenerated IVDs, as well as a non-uniform distribution of IDP across the entirety of the IVD.[7,11,24] The loss of hydration also causes the annulus fibrosus to decrease in height.[29] These alterations in composition and morphology have a direct impact on the mechanical properties of the IVD, and thus may in turn affect loads transmitted to adjacent vertebrae.

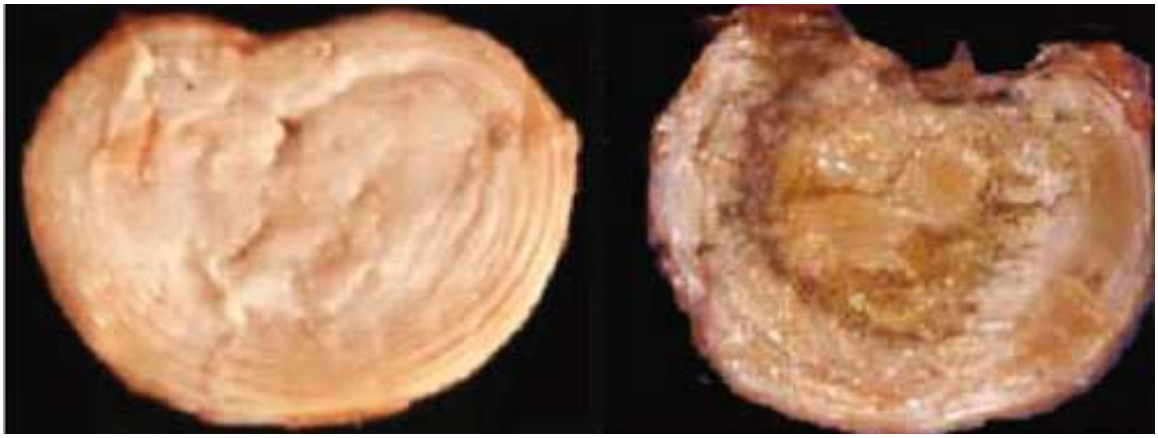

Figure 1.3 Mid-transverse slices of normal (left) and severely degenerated (right) IVDs.[23]

Numerous methodologies have been developed to assess, or grade, IVD degeneration. Past systems, such as the Thompson grading scale, have utilized transverse[30], or sagittal sections[31] to categorize varying levels of degeneration based on gross (*i.e.*, macroscopic) examination of the internal anatomy of the IVD. In addition, non-invasive assessments of disc degeneration based on various imaging modalities have been established. Lateral radiographs have been utilized to categorize levels of IVD degeneration based on IVD height and the presence of osteophytes.[32] Methods, such as

the Pfirrmann grading scale, utilizing magnetic resonance imaging (MRI) to grade mid-sagittal images of IVDs have also been developed.[33–35] In general, the grading scheme that use gross examination of tissue sections or MRI categorize levels of degeneration according to the extent of homogeneity of the NP region and the clarity of the border between NP and AF. Recently, a quantitative computed tomography (QCT) –based grading scale, termed "apparent loss of disc integrity" (ALDI) has been developed to grade degeneration of the IVD.[21] The ALDI grading scale is primarily based on the ability to distinguish a boundary between the NP and surrounding AF of mid-transverse QCT images of the IVD. In a QCT image, healthy IVDs exhibit a dark, centralized NP as a result of high water content. Primary indicators of degeneration include the loss of differentiability between the NP and AF regions, and the appearance of fissures within the tissue of the IVD. The presence of osteophytes within the IVD tissue is a secondary indicator of IVD degeneration.

CHAPTER TWO

PRELIMINARY STUDIES: DEVELOPMENT OF MECHANICAL TEST APPARATUS AND INSTRUMENTATION

COMPLETED IN COLLABORATION WITH ALEXANDER M. ADAMS AND KAMIL K. MAKHNEJIA PER REQUIREMENTS OF THE BOSTON UNIVERSITY DEPARTMENT OF BIOMEDICAL ENGINEERING SENIOR PROJECT 2014

INTRODUCTION

The use of pressure transducers has been well documented in the literature as a means of accurately measuring intradiscal pressures.[8,9,10,14] In order to facilitate accurate, controlled insertion of a pressure transducer throughout loaded intervertebral discs (IVDs), an assembly compatible with the platform of a servohydraulic test frame was manufactured. Specialized fixtures to accommodate specimen geometry and provide the necessary loading scenarios within the test frame were also manufactured.

ASSEMBLY

In this section, the design and manufacture of the mechanical test apparatus and the associated instrumentation utilized for the study are discussed.

Circuitry and Instrumentation

Pressure measurements were collected through the use of a high-pressure needle pressure transducer (Gaeltec Ltd., Dunvegan, Isle of Skye, UK). The device consisted of a 4F (1.33mm diameter), 100mm-long domed steel needle embedded with a 5mm x 1mm pressure transducer located 5mm from the distal end of the needle (Figure 2.1). Calibration of the pressure transducer was done by the manufacturer, and established a full-scale range of 0–3MPa gauge pressure with sensitivity of 0.66-μV/V/kPa. Insertion and retraction of the needle pressure transducer throughout the disc during testing was

achieved through the use of a linear actuator (Firgelli Automations, Ferndale, WA, USA). The actuator also incorporated a 0–10kΩ potentiometer, which allowed for position sensing of the pressure transducer throughout testing. Upon procurement of the actuator, the potentiometer was tested to ensure linearity of the resistance change relative to position (Figure 2.2).

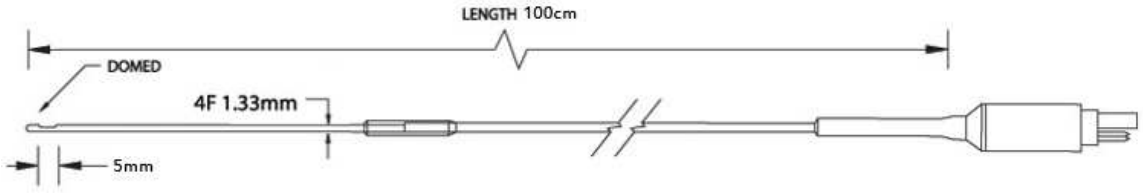

Figure 2.1 Schematic drawing of high-pressure needle pressure transducer. Image courtesy of Gaeltec Ltd.

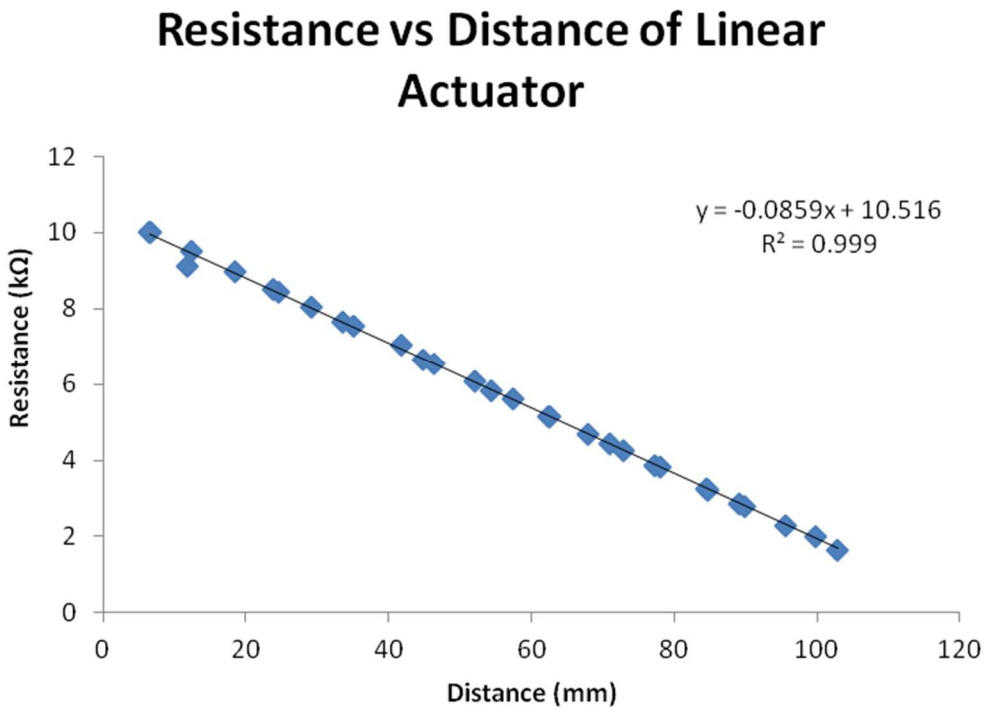

Figure 2.2 Potentiometer resistance versus extension distance of a linear potentiometer.

A data acquisition board (myDAQ, National Instruments, Austin, TX, USA) was used both to capture output voltage data from the pressure transducer and potentiometer and to provide excitation voltages for the instruments. In order to integrate the instrumentation and monitor their outputs in real-time, a LabVIEW (National Instruments, Austin, TX, USA) program was created (Figure 2.3). The program utilized a graphical user interface, plotting both distance and pressure at a sampling rate of 1 kHz. A third plot was generated that displayed the measured gauge pressure vs. pressure transducer position within the IVD. In doing so, the operator was able to have precise positioning control of the actuator, which advanced the transducer through the IVD, and allowed the operator to visually confirm that the pressure transducer had left the disc space. All plots were continuously updated throughout the experimentation procedure, and displayed up to 20s of previously collected data. A separate calibration LabVIEW program was also utilized prior to each test (Figure 2.4). The output signal at two actuator positions—completely retracted and fully extended—was captured, followed by the DC offset of output from the pressure transducer. The program automatically calculated and saved calibration coefficients to be referenced by the data acquisition program, such that the output signals from both the actuator and pressure transducer could be converted to physical units.

In order to convert the change in resistance of the linear potentiometer to a change in voltage output, a Wheatstone bridge circuit was constructed that receives a 1V excitation voltage and outputs a voltage linearly proportional to the distance change of the actuator.

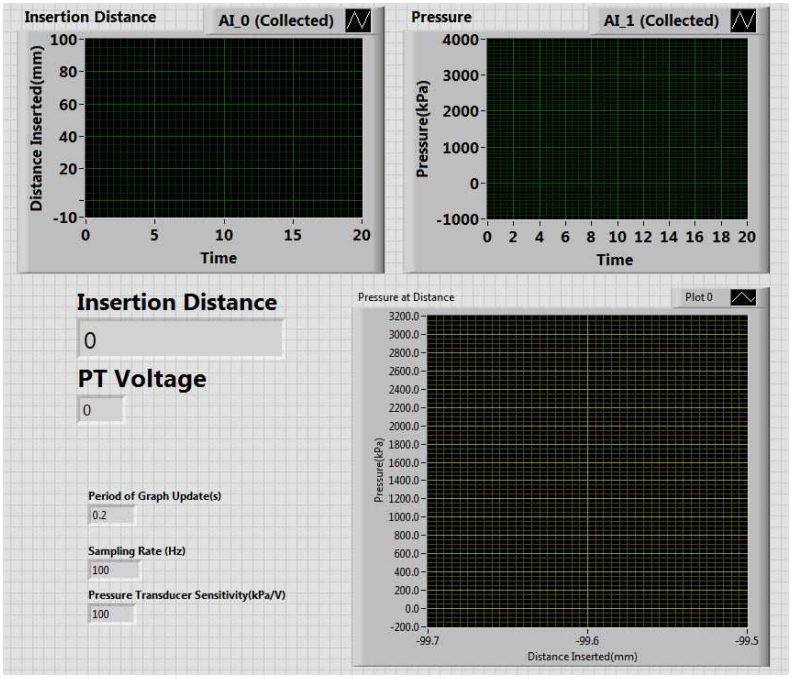

Figure 2.3 LabVIEW user interface displaying needle pressure transducer distance within the IVD (top left), intradiscal pressure (top right), and a pressure vs. distance (bottom right).

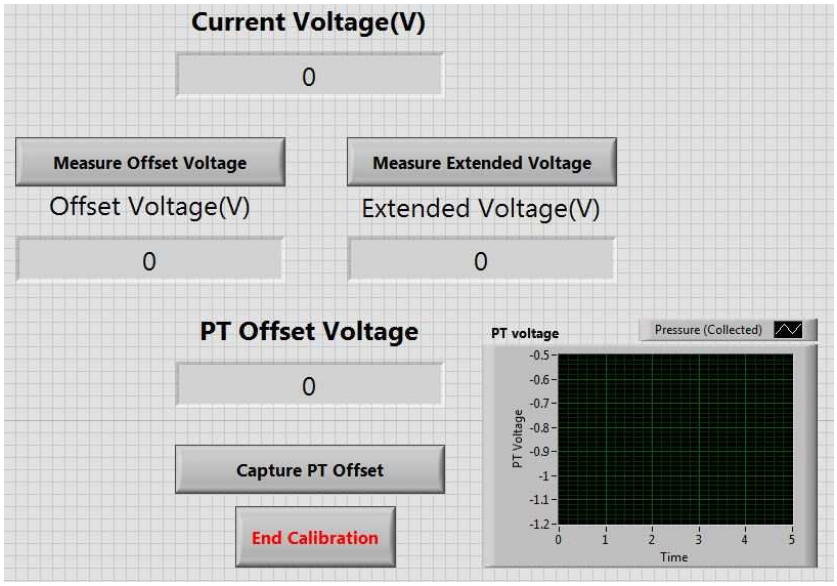

Figure 2.4 LabVIEW user interface for calibration of the linear potentiometer, capturing voltages at both completely retracted and fully extended positions. Values obtained from the calibration were saved and applied to the data collection program.

The sensitivity of the pressure transducer is less than 1μV/kPa; therefore, the pressure transducer's output at full-scale range (3 MPa) is less than 3mV. Thus it was critical that the signal from the pressure transducer be amplified by a large linear gain to utilize a larger portion of the data acquisition board's full-scale range. A simple instrumentation amplifier circuit was used. The circuit utilized μA741 General-Purpose Operational Amplifiers (Texas Instruments, Dallas, TX, USA), powered with ±15V from the data acquisition board. The amplifier used for data collection was tested prior to use in order to determine the exact linear gain of 105V/V with negligible uncertainty.

Due to the relatively small amplitude of the pressure transducer signal prior to amplification, this instrument is subject to noise from surrounding electronics and machinery. A simple low-pass filter with a cutoff frequency of 50 Hz was installed in the circuitry to reduce noise at 60Hz allowing the pressure to be visualized on the LabVIEW interface.

Power and control of the of the linear actuator was achieved with an adjustable DC voltage supply and a circuit that allows the user to turn power to the actuator on and off as well as to control the direction of the voltage applied to the actuator. This circuit used a push button gate in series with a double-pole, double-throw (DPDT) switch wired to allow for voltage direction switching, and thus forward and reverse motion of the actuator.

Manufacture of Linear Actuator / Pressure Transducer Assembly

A mechanical device was manufactured to support the linear actuator and needle pressure transducer throughout testing. The device needed to achieve proper alignment

with four degrees of freedom: (1) height adjustment in the superior-inferior direction, (2) adjustment in the anterior-posterior direction (partially accommodated by the linear actuator), (3) angle adjustment in the transverse plane, on the surface of the servohydraulic test frame platform (Instron 8874, Canton, MA, USA), and (4) angle adjustment in the sagittal plane (Figure 2.5).

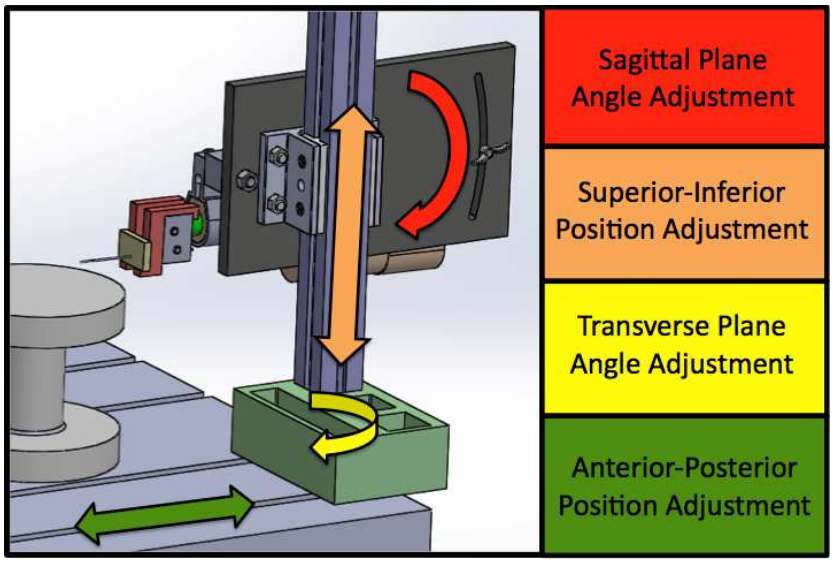

Figure 2.5 SolidWorks model of linear actuator-pressure transducer assembly showcasing the motion capabilities of the device.

A base plate component was milled from a 6x4x2” stock bar of 6061 aluminum (Figure 2.6). The base plate supports the upper portion of the device, while also facilitating both anterior-posterior translation and rotation in the transverse plane on the Instron test frame platform. A counterbore slot was machined into the part using computerized numerical control (CNC) milling to allow for adjustability via the existing T-slot/T-nut mechanism present within the platform of the Instron test frame. Three additional, square counterbore slots were machined into the part to give flexibility for the

location of the aluminum support of the device.

The device utilized a bar of extruded structural aluminum and a linear bearing brake kit (80/20 Inc., Columbia City, IN, US) to achieve the required superior-inferior adjustments necessary for pressure transducer insertion during testing, and to support the weight of the linear actuator (Figure 2.6). During the testing of a single sample, it is required that both superior and inferior IVDs are tested. Incorporation of the manually operated linear brake system allows for quick adjustment to achieve correct insertion height with minimal backlash.

A track plate was CNC-milled out of ABS plastic to support the linear actuator and offer adequate angular rotation of the unit in the sagittal plane (Figure 2.6). The front end of the actuator was pin mounted to the track plate, while the back end was fastened to an adapter piece and connected to the track plate through the use of a wing nut situated within a curved track. This method of fixing the actuator allowed for manual adjustment of the necessary insertion angle through the IVD as defined by analyzing projected 2-D slices of the test samples.

Synchronous motion of the pressure transducer during forward and reverse actuation was achieved through the use of a CNC-milled aluminum adapter (Figure 2.6). This piece fits around the distal end of the actuator shaft and is fastened through the provided clevis hole. The adapter acts to facilitate insertion and retraction of the needle pressure transducer and to prevent the needle from buckling under applied loads.

A concentric cannula was obtained in order to guide and protect the needle pressure transducer throughout the IVD (Eagle Stainless Tube & Fabrication Inc.,

Franklin, MA, USA). The sliding fit tolerance between the cannula and the transducer allowed for easy cannula retraction and prevented excessive tissue buildup between the two. The cannula featured a sharpened double bevel tip that acted as a cutting tool to provide a clear path for the pressure transducer, and was attached to a clearance hole in a ¼" 6061 aluminum stock plate through the use of PERMABOND® 910 metal bonding agent (Figure 2.7). This plate was used to retract the cannula following full insertion of the needle pressure transducer within the IVD. The insertion of this transducer-cannula system into the IVD as a rigid unit was made possible by the use of aluminum spacer components, which kept the sharpened tip ahead of the distal end of the needle. Upon reaching the desired insertion depth within the IVD, these spacers were removed, and the cannula plate could be retracted, thus exposing the pressure transducer window for subsequent data collection.

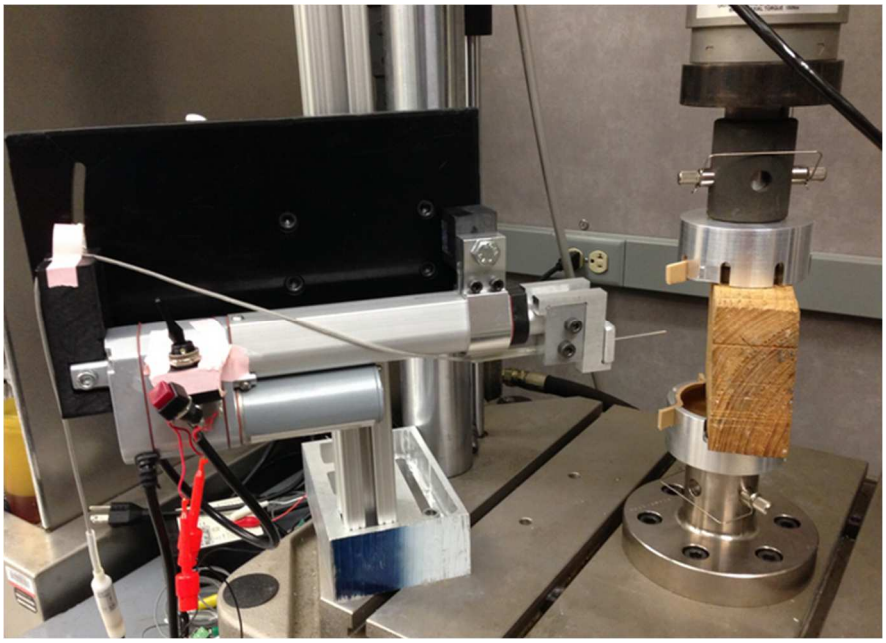

Figure 2.6 Linear actuator and pressure transducer assembly, shown with angular adjustment track plate, base plate, extruded aluminum support, and custom-manufactured test platens integrated within the test frame.

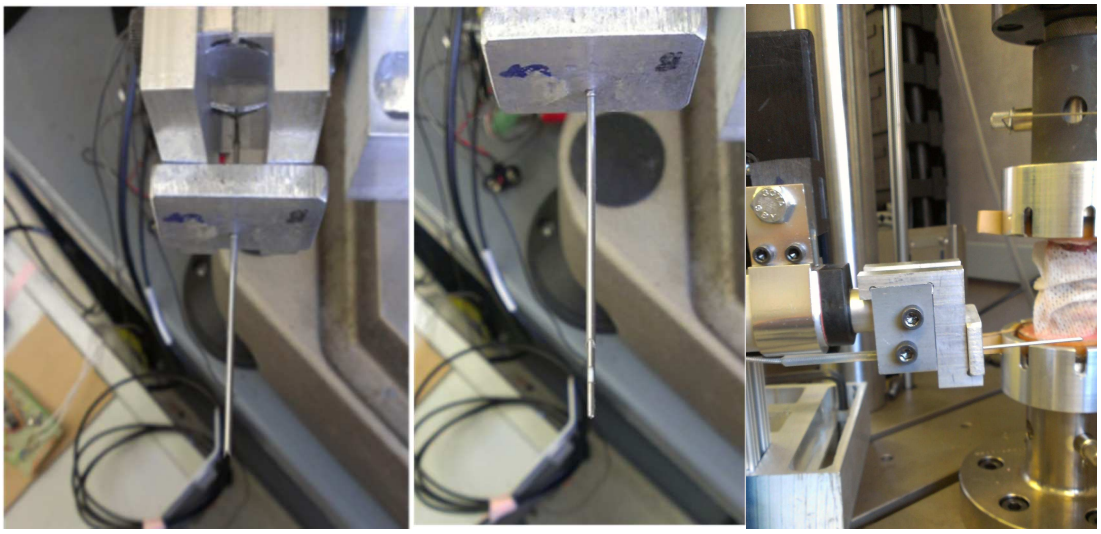

Figure 2.7 Double-bevel-sharpened cannula and aluminum stock plate in extended insertion position (left) and retracted position for data collection (center). L-shaped spacer brackets keep the sharpened tip of the cannula ahead of the pressure transducer during insertion, and are removed for retraction of the cannula and exposure of the pressure transducer window (right).

Manufacture of Axial Compression / Anterior Flexion Test Fixture Platens

In order to achieve the necessary loading conditions for this study, custom platens were manufactured out of a 6061 aluminum rod stock via CNC-lathe to integrate with the existing Instron test frame. Samples in this study are either tested in axial compression or axial compression with an applied 5° anterior flexion. The platen assembly is comprised of two components: (1) a cup-shaped outer component to apply force onto the test subject, and to accommodate ULTEM potting trays within during testing, and (2) removable cylindrical inserts that provide either 2.5° anterior flexion or 0 degrees of anterior flexion. Samples are preselected for either axial compression or axial compression with 5° anterior flexion prior to testing, allowing the researcher to install the correct cylindrical insert based on the given test (Figure 2.8).

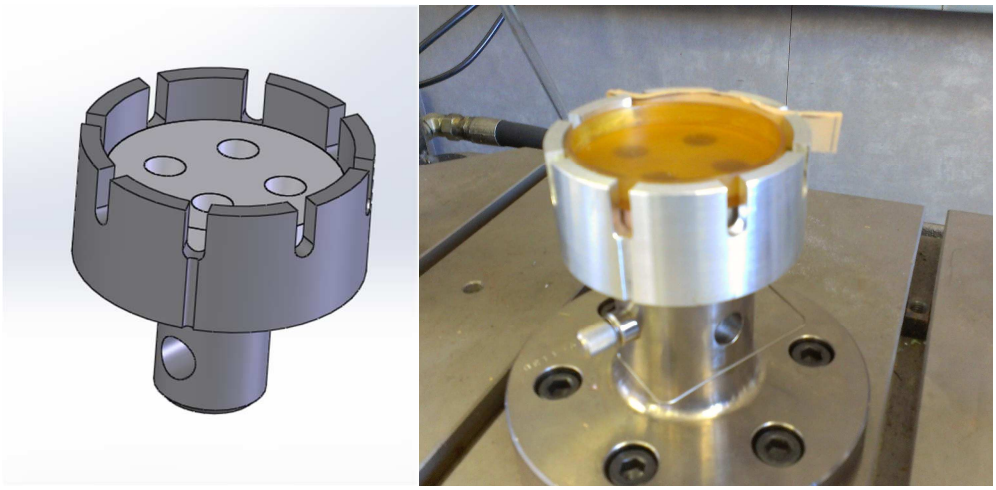

Figure 2.8 Custom platens for testing shown as SolidWorks 3D model (left) and integrating with the existing Instron test frame (right).

VALIDATION

Polydimethylsiloxane (PDMS) Proof-of-Concept Testing

Polydimethylsiloxane (PDMS) cylinders were fabricated to conduct proof-of-concept testing. The PDMS cylinders were used as substitutes for IVDs, to ensure proper function of the mechanical device, pressure transducer, and stainless steel cannula assembly prior to insertion and data collection within real human cadaveric IVD samples. The conventional PDMS fabrication technique utilizing a 10-to-1 proportion between the base and curing agents was altered to increase the curing agent concentration to a 5-to-1 proportion. The larger amount of cross-linking agents yielded PDMS stiffness values in the 3–5 MPa range, the worst-case scenario for degenerated IVDs. The 5-to-1 solution was poured into an aluminum mold (50 mm diameter, 38 mm height) and placed for roughly 20 minutes in a vacuum chamber where the pressures were quickly cycled to burst surface air bubbles. Afterwards, the mold was placed in an oven at 60°C for two hours and at room temperature for 48 hours. Finally, with the completion of the curing stage of the fabrication process, the PDMS samples were removed by disassembling the mold. During testing, the transducer-cannula assembly was inserted and drawn out of these PDMS cylinders in a fashion similar to that used in the cadaveric IVD samples, providing both an excellent baseline approximation of data acquisition, and elucidating any major complications that arose between the pressure transducer and cannula. The pressure transducer was inserted into the PDMS cylinder subject to a 500N compressive load. It pierced the material with ease and retracted without stalling the actuator. Some minor adjustments to the testing apparatus were made with feedback from this test. These

adjustments included adding a rigid cannula support in the form of a fabricated aluminum retraction plate, and adjustment to the cannula tip profile to prevent excessive deflection.

Lumbar Vertebrae Proof-of-Concept Testing

As a preliminary test to further ensure functionality of the mechanical and electrical systems, a lumbar spine segment (L2–L4) was used for testing. Compared to the actual thoracic test samples, this preliminary test sample lacked posterior elements to allow easier identification of the trajectory of the pressure transducer. Although lower thoracic spine levels were of interest in this study, the lumbar region of the spine was chosen for the preliminary test sample because the IVDs in this region are larger than the discs of the thoracic region, and the risk of pressure transducer damage is greatly decreased. For the validation of experimental procedures and functionality of the mechanical and electrical systems, the large healthy sample proved sufficient as a preliminary model. Before mechanically testing the sample and collecting pressure data, the spine segment was submerged in a water bath for an hour to ensure proper thawing of the entire fresh frozen segment. After thawing, the sample was loaded into the custom-fabricated Instron platens. Consequently, the angled platen inserts were oriented to allow for sufficient anterior flexion. The preliminary test sample was flexed a total of five degrees and axially compressed with a load of 700N. Although the sample and loading conditions were different for the preliminary testing as compared to actual testing, the data collection methodologies–i.e. insertion, retraction and subsequent data collection–were followed as described for testing lower thoracic samples. Although not graded with ALDI scoring, the disc appeared to be healthy with a large disc space. Intradiscal

pressure was collected along the mid-sagittal path (Figure 2.9). Along the paths, as seen in the figure below, the pressure transducer was not passed entirely through the disc. This limitation was the result of two factors: 1) supporting extra length of the needle to ensure safety throughout the process and thus shortening the length available to pass through the IVD; and 2) not accounting for the larger mid-sagittal cross-section of the lumbar IVD, in comparison to that of a thoracic IVD. A sharp rise in pressure is noted in the anterior AF region (A), with average pressure in the central region between 600 and 700kPa, before starting to decrease in the posterior AF region (P). These values are expected for an applied load of 700N, due to the large cross-sectional area of the IVD.

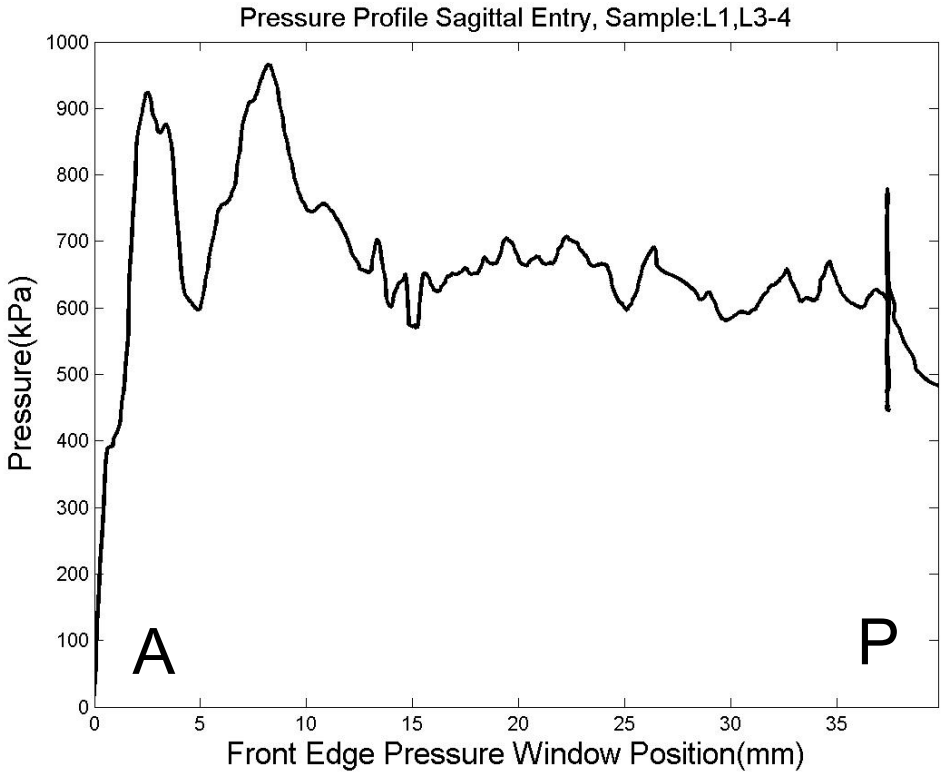

Figure 2.9 Preliminary intradiscal pressure measurement along the mid-sagittal path of an L3–L4 IVD, shown from anterior (A) to posterior (P) from left to right.

CHAPTER THREE

SPATIAL MAPPING OF PRESSURE WITHIN THE INTERVERTEBRAL DISC

INTRODUCTION

Degeneration of intervertebral discs is strongly associated with back pain[10] and affects approximately 60% of the population by age 70.[9] Given that the intervertebral disc is a primary load-bearing structure in the spine, measurement of the changes in intradiscal pressure (IDP) that accompany disc degeneration are a clear, functional measure of the disease pathology. Indeed, *ex vivo* studies have found a loss of IDP overall and changes in the spatial distribution of pressure within the disc with increasing levels of disc degeneration.[20] However, few studies of IDP assess disc degeneration by non-invasive means.[36] In addition, the pressure measurements are typically performed at a single location within the disc or along only a single linear path (e.g., mid-sagittal line) through the disc. The overall goal of this study was to determine the correspondence between the spatial distributions of IDP, as measured along both mid-sagittal and mid-coronal paths, and a clinically feasible assessment of disc health. The specific objectives were: 1) to quantify the IDP in regions corresponding to the nucleus pulposus (NP) and annulus fibrosus (AF) and to determine whether the regional dependence of IDP varies with disc degeneration; and 2) to quantify the heterogeneity in IDP within the NP and AF and the dependence of this heterogeneity on disc degeneration.

METHODS

Specimen Preparation

Twenty-six thoracic spine segments consisting of three vertebrae and interstitial IVDs (eight T9–T11 and eighteen T10–T12; NDRI, Philadelphia, PA, USA and Life

Legacy Foundation, Tucson, AZ, USA) were dissected from fresh-frozen human spines (age: 35–86 years, mean ± standard deviation: 68 ± 16; 16 male, 10 female). Transverse cuts were made through IVDs adjacent to the top and bottom vertebrae of the segment just above their respective vertebral endplates, and all of these flanking IVD tissues were removed. The top and bottom vertebral endplates of each segment were potted in circular, radiolucent dishes filled with polymethyl methacrylate (PMMA), such that the posterior elements were not fixed, allowing for more physiologic transfer of load throughout the segment via the zygapophysial joint (Figure 3.1). Spine segments were kept hydrated throughout preparation and during testing by phosphate buffered saline (PBS) solution soaked gauze. The spine segments were sealed in plastic bags and stored at -20 °C when not in use.

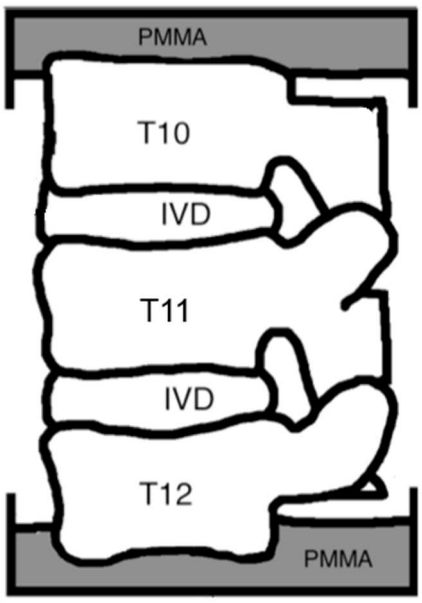

Figure 3.1 Schematic drawing of T10–T12 spine segment used for testing. Image courtesy of Timothy Jackman.

Sample Imaging and Disc Grading

Each segment was imaged using quantitative computed tomography (QCT) performed with a LightSpeed VCT CT system (GE Healthcare, Cleveland, OH, USA) at Boston Medical Center. Scans were carried out at one of two resolutions (1) 0.3215×0.3125×0.625 mm/voxel and (2) 0.3906×0.3906×0.625 mm/voxel. For both resolution scans, the voltage, current, and scan field of view settings were as follows: 120kVp, 240mA, and 32mm, respectively. The use of two scan resolutions was a result of operator error. Prior to testing, the QCT data were analyzed using an image-processing program (ImageJ; NIH, Bethesda, MD, USA), and projected into 2-D frontal and sagittal slices. Relevant 2-D slices of the IVDs were consulted in order to identify potential abnormal intradiscal osteophytes that could cause damage to the pressure transducer. Additionally, mid-sagittal and mid-coronal distances and IVD tilt angles were measured across the disc space (Figure 3.2), and compiled using a MATLAB script (MathWorks, Natick, MA, USA). These data were referred to throughout the mechanical testing procedure for accurate positioning of the pressure transducer through the disc space.

Transverse QCT slices were used to score IVDs based on their level of degeneration, utilizing the "apparent loss of disc integrity" (ALDI) method previously developed.[21] The presence of a well-defined boundary between a dark, centralized nucleus pulposus and annulus fibrous are representative of a healthy IVD. A decrease in ability to detect the boundary between nucleus pulposus and annulus fibrosus, as well as the appearance of fissures, calcifications or osteophytes indicate degeneration within the IVD. The discs were graded by an independent observer (Timothy Jackman) on a scale

of 0 (no or mild degeneration) to 2 (severe degeneration) prior to subsequent pressure measurement (Figure 3.3). Furthermore, the mid-transverse slice of each IVD was contoured in order to calculate the cross-sectional area of the disc.

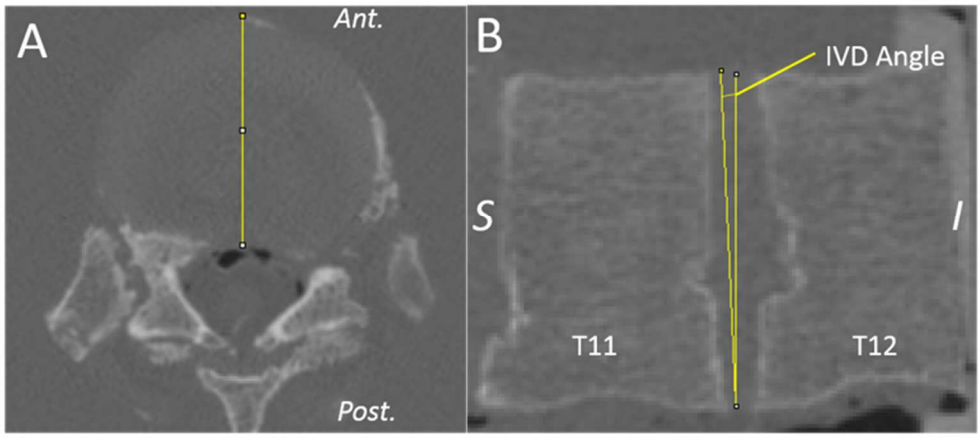

Figure 3.2 (A) Mid-transverse QCT image slice used to measure anteroposterior distance across the IVD and (B) mid-sagittal slice used to measure IVD tilt angle, to aid in accurate transducer insertion. Images processed using ImageJ.

Table 3.1 Distribution of IVDs based off of loading condition and ALDI score.

	ALDI Score		
Loading Condition	*ALDI 0*	*ALDI 1*	*ALDI 2*
Axial Compression	8	8	8
Anterior Flexion	9	9	9
TOTAL	**17**	**17**	**17**
	= 51 IVDs		

*: One superior IVD (given ALDI 2 grade) was excluded from testing due to presence of large, bridging osteophytes preventing transducer insertion.

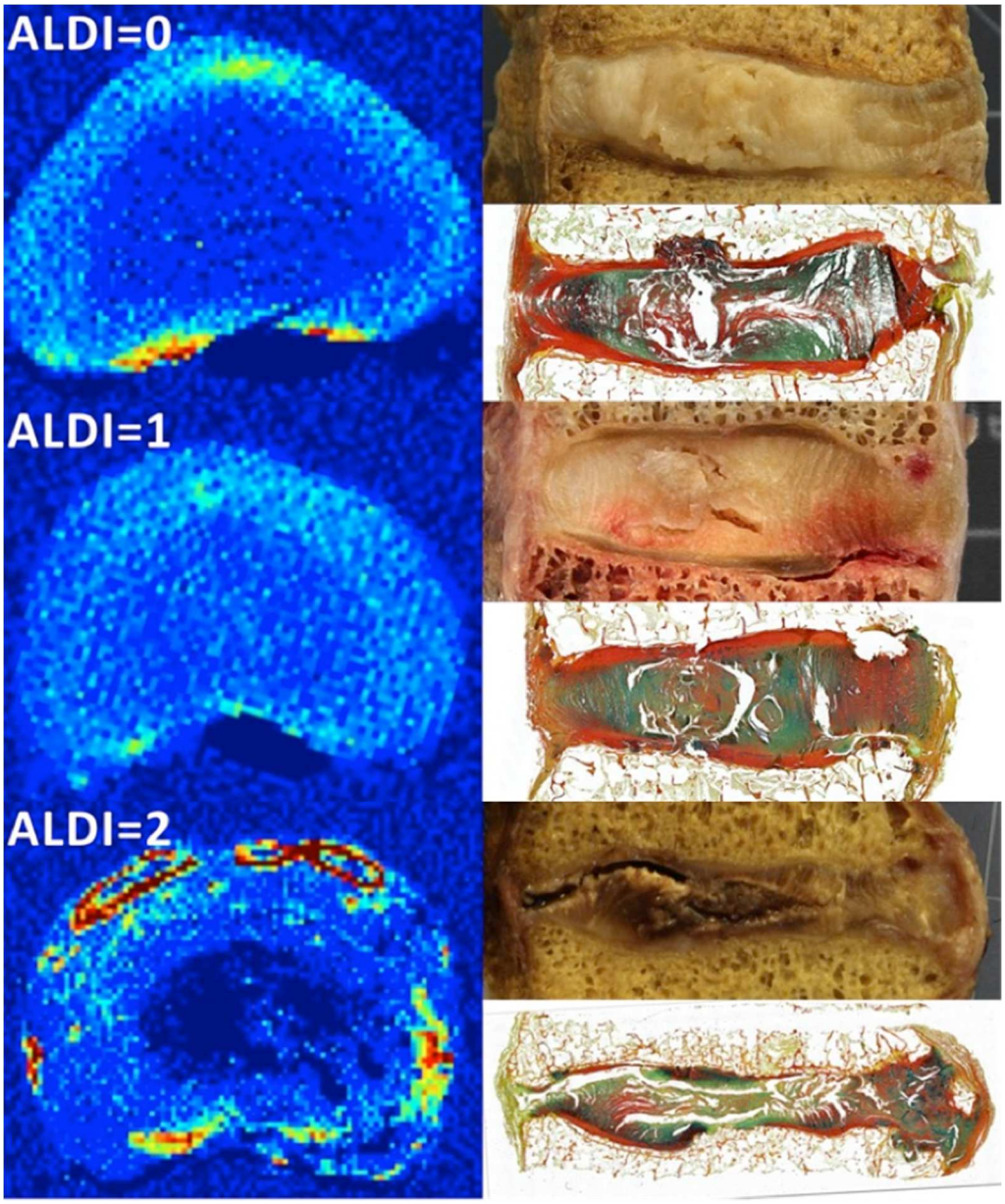

Figure 3.3 ALDI grading scale. Shown at the left of the three rows are transverse QCT slices of the IVD are shown with ALDI scores at the top left. The red orange and yellow regions represent portions of the endplates and calcifications within the tissue; however, no osteophytes are present in the QCT images shown above, but rather portions of endplate from adjacent vertebrae.[21] Shown at right of each row are corresponding optical images (top right) and histological sections (bottom right) for a mid-sagittal cross section of the IVD.

Mechanical Testing

Prior to testing, specimens were thawed in PBS for one hour, changing the surrounding warm water bath once after the first half hour. The specimens were then affixed to the custom-manufactured platens on the servohydraulic test frame (Instron 8874, Canton, MA, USA), and subject to a compressive preload of 300N for 30 minutes to combat post-mortem superhydration effects.[12] After this preload, samples were then subjected to a 500N load, randomly assigned to either axial compression (n=12 samples) or axial compression with applied anterior flexion (5°; n=14 samples). For samples subject to the latter, angled platen inserts were installed in such a way that flexion was applied anteriorly. Pressure measurements were made by inserting a needle pressure transducer through the entirety of the IVD and then collecting data during retraction at a rate of approximately 1mm/sec, along both mid-sagittal and mid-coronal paths. Pressure and position data were collected at a frequency of 1 kHz. One superior IVD was excluded from this data collection, due to the presence of bridging osteophytes preventing insertion of the transducer through the disc space.

Regional Morphometric Analysis and Calculation of Regional IDP

After collecting IDP for each of the samples, a MATLAB program was utilized to align the pressure profile to a QCT image corresponding to the sample IVD and path (Figure 3.4). The intradiscal structures of these IVDs were visualized alongside the profiles, allowing for the placement of points on landmarks of the intervertebral disc: the edges of the AF, and the apparent boundaries between AF and NP. This allowed for the separation of each path into three intradiscal regions (anterior AF, NP, posterior AF for

the mid-sagittal path; left AF, NP, right AF for the mid-coronal path). For severely degenerated discs in which the boundary between NP and AF was unclear, the NP region was defined as a region of the pressure profile located between anterior and/or posterior peaks wherein variations in pressure were less than or equal to 10%, as described in literature[11] . Four such IVDs required the use of this approximation, all of which received an ALDI score of 2. The NP width of these four samples needing approximation all were within a range of 10–20% of the total distance across the IVD.

The mean IDP in each region was calculated. The spatial heterogeneity, $\boldsymbol{R_a}$, in IDP within each region was quantified by the average absolute deviation from the regional mean, using the following equation:

$$R_a = \frac{1}{N}\sum_{i=1}^{N}|(y_i - \bar{y})| \qquad \text{Eqn 3.1}$$

where N is the number of points in a given region, y_i is the IDP at point i, and $\bar{y}$ is the mean value of the IDP in the region (Figure 3.5). The maximum value of IDP in each of the anterior and posterior AF regions, and in each of the left and right AF regions was recorded. The slope of the line drawn between the regional maximum and the edge of the nucleus average nearest to the anatomical site was defined as the gradient, as previously characterized. However, this study utilized the average nucleus pressure at the boundary between AF and NP as opposed to the edge of a "functional nucleus" (Figure 3.6).[20] Samples in which the slope of the stress gradient was found to be infinite were excluded from statistical analysis.

IVD Correction Factor for Finite Element (FE) Models

The measured intradiscal pressure across the NP region was also used to establish a correction factor for given thoracic IVDs for use in finite element models. The correction factor, C_{ind} is utilized to give an approximation of the compressive force, $\tilde{F}_{compr}$ acting on an intervertebral disc, given by the following equation:

$$\tilde{F}_{compr} = p_{intr} \times A \times C_{ind} \qquad \text{Eqn 3.2}$$

Where p_{intr} is the intradiscal pressure measured at a single point within the NP, and A indicates the cross-sectional area of the IVD (Figure 3.7)[30,37] In this study, p_{intr} was defined as the average intradiscal pressure measured across the entirety of the NP. The actual compressive force applied to the spine segment, F_{compr}, was established at 500N and thus could be substituted into the following equation, to calculate the IVD correction factor[37]:

$$C_{ind} = \frac{F_{compr}}{p_{intr} \times A} \qquad \text{Eqn 3.3}$$

Average C_{ind} values were calculated for IVDs of varying ALDI scores, under varying loading conditions and pressure transducer paths. In addition, C_{ind} values were calculated using p_{intr}as the average intradiscal pressure measured across the entirety of the IVD, for comparison.

Statistical Analyses

To enable comparisons among samples, the values of IDP were multiplied by the cross-sectional area of the disc, measured on a mid-transverse image of the disc. Repeated-measures analysis of variance (ANOVA) with ALDI score as the between-

subjects factor and region as the within-subjects factor were carried out for each combination of loading condition (compression or compression with flexion) and path. Average regional intradiscal loads were used as the dependent variable. Additionally, comparisons of ALDI scores to sample body weight ($p>0.520$) and sample BMI ($p>0.621$) revealed no experimental bias within the data set; ALDI scores were not found to be preferential to a high or low body weight or BMI. Analyses were performed using JMP v11.0 (SAS, Cary, NC, USA). Significance was accepted at the 5% level.

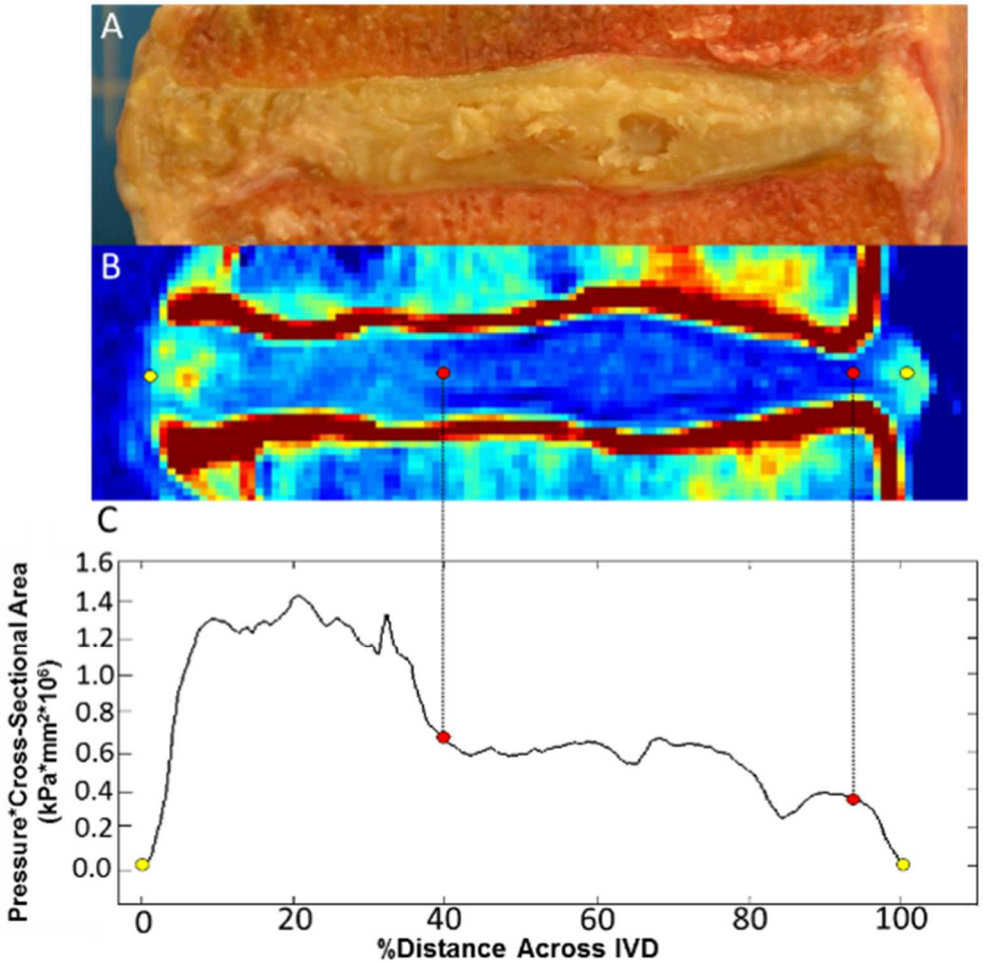

Figure 3.4 Mid-sagittal cross section (A) and morphometric analysis utilized to divide IDP profile into annulus fibrosus and nucleus pulposus regions (B, C).

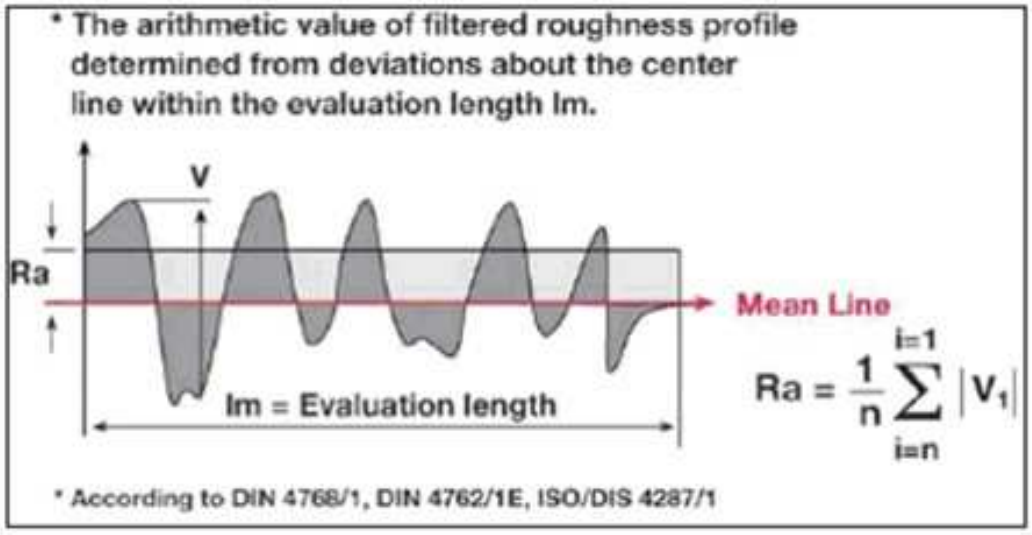

Figure 3.5 Example of average absolute deviation from the mean equation utilized to determine spatial heterogeneity of IVD pressure load distribution. Image courtesy of Applied Industrial Technologies, 2006.

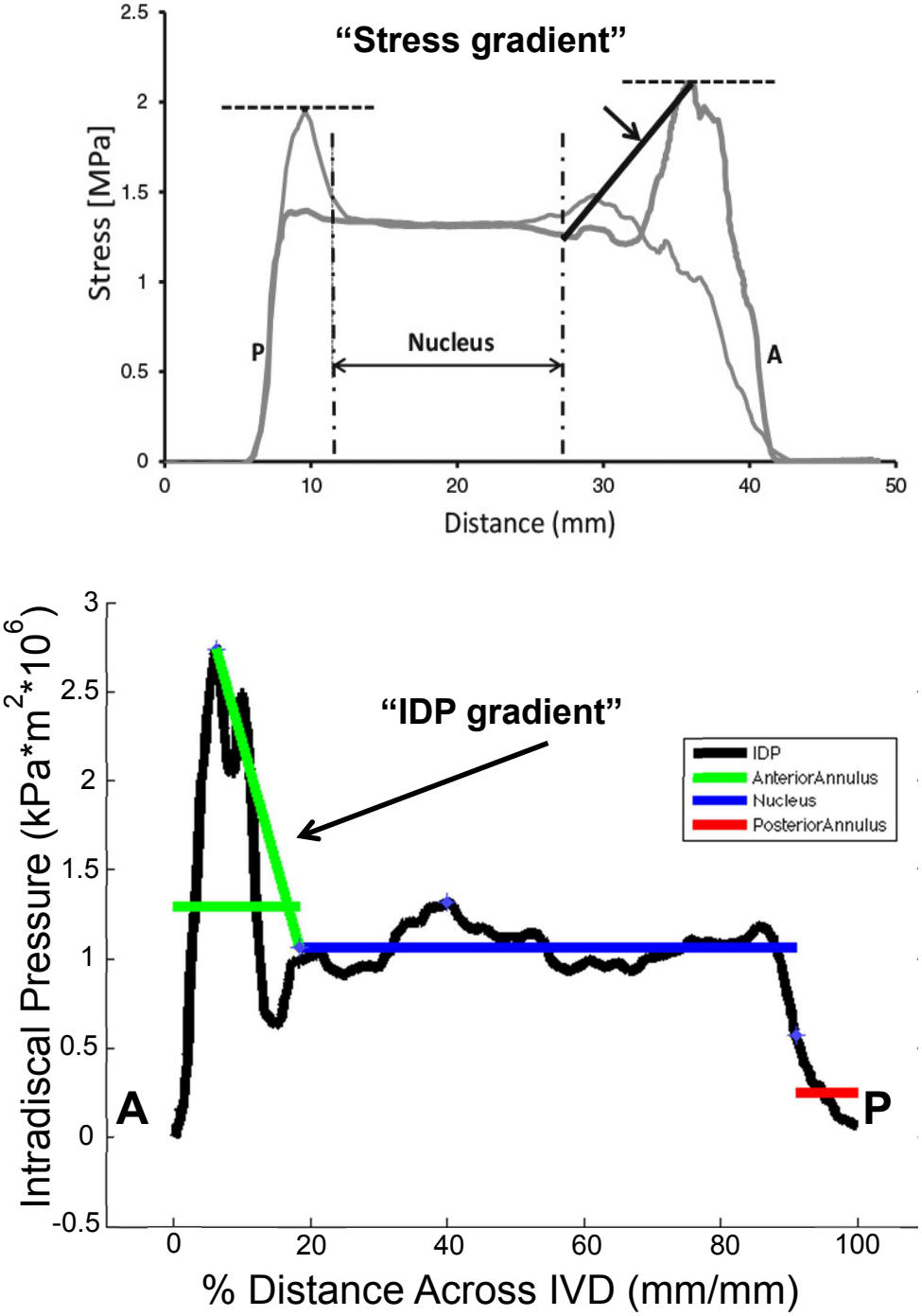

Figure 3.6 Diagrams representing the determination of "stress gradients" based on the slope between peak stresses in the annulus region and adjacent edge of a "functional nucleus,"[20] (top) and the determination of "IDP gradient", based on the slope between

peak loads in the annulus region and the adjacent edge of the morphometry-defined average nucleus load (bottom).

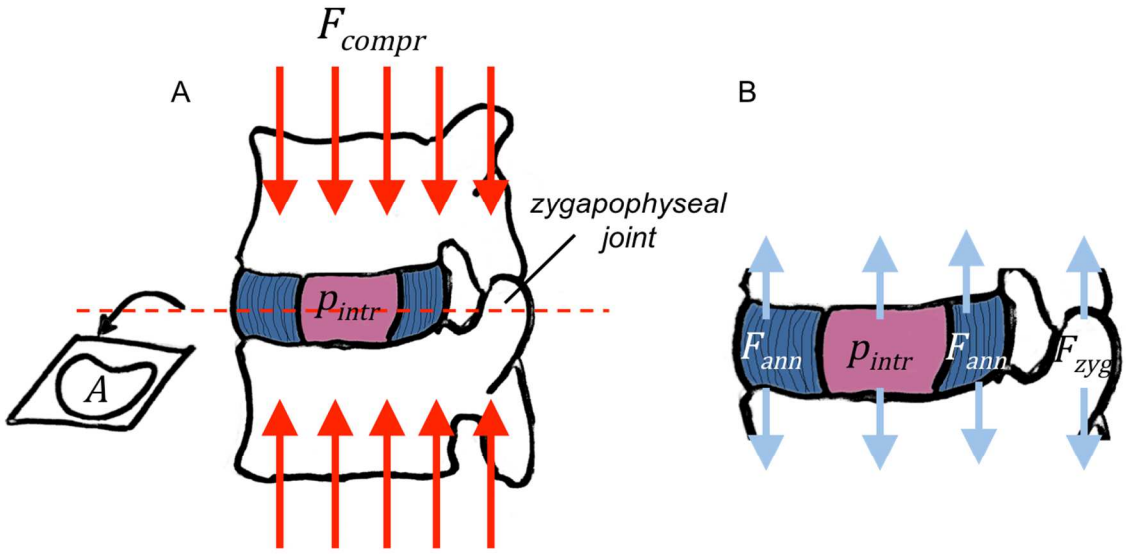

Figure 3.7 Schematic mid-sagittal drawing representing the measurement of the applied compressive force F_{compr}, the IDP within the NP region, p_{intr}, and the cross-sectional area of a mid-sagittal slice of the IVD, used to generate a correction factor for approximating compressive force on an IVD in FE models (A) and forces across the IVD—annular forces, F_{ann}, IDP p_{intr}, and the forces exerted on the zygapophysial joint, F_{zyg}—that together counteract F_{compr} (B).

RESULTS

Average Regional IDP

For segments loaded in axial compression, mean IDP was higher in the in the NP as compared to the posterior AF ($p=0.008$; Figure 3.8). Within-subjects analysis of intradiscal region revealed no significant differences between left AF, NP or right AF ($p=0.136$; Figure 3.8).

For segments loaded in axial compression with an applied 5 degrees of anterior flexion, mean IDP was higher in both the anterior AF and NP when compared to the posterior AF ($p<0.004$; Figure 3.9). No dependence of these regional differences on ALDI score was found ($p>0.374$); however, for all three regions in the sagittal path combined, mean IDP (normalized by cross-sectional area) was higher for ALDI score 0 vs. 2 ($p=0.044$).

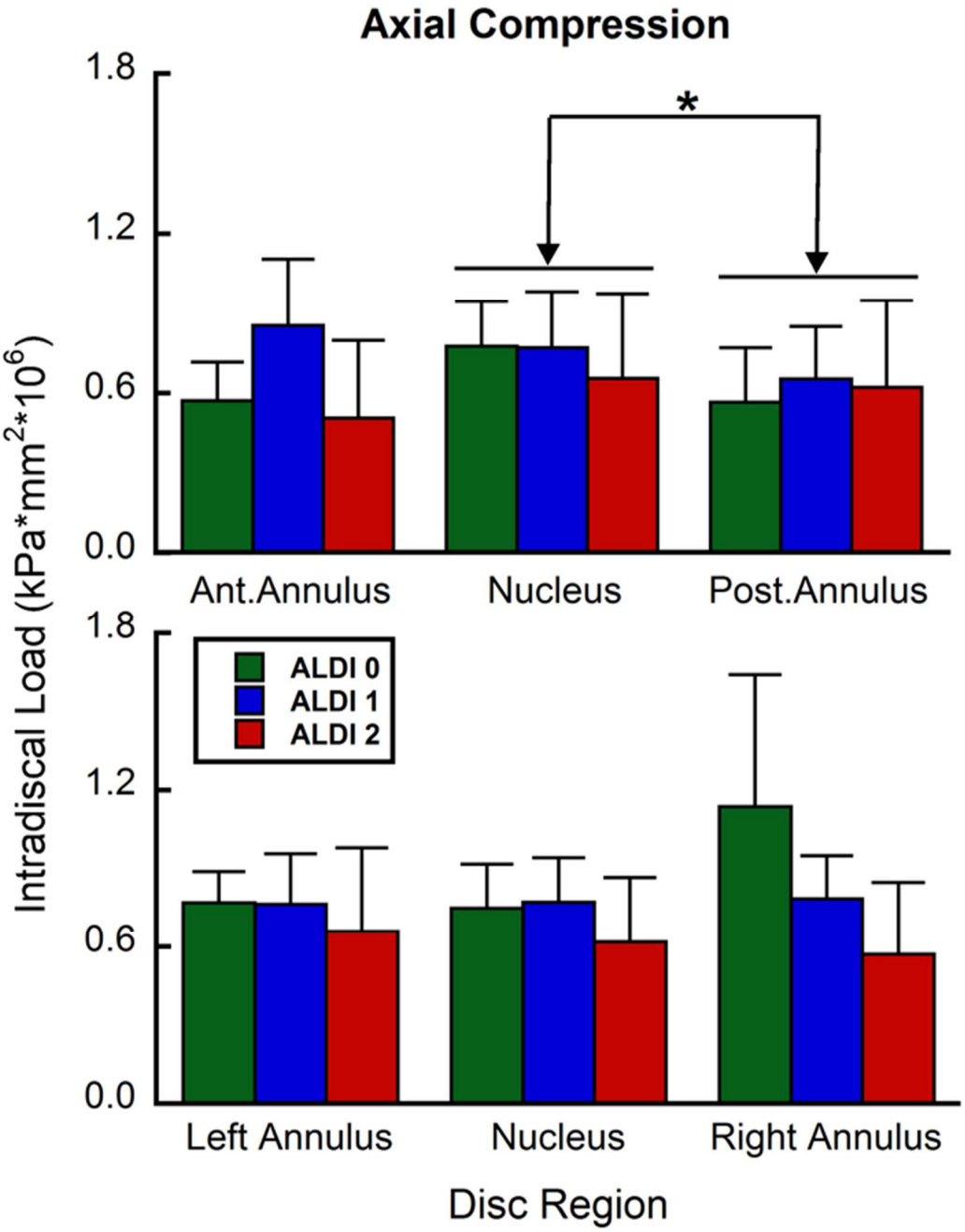

Figure 3.8 Mean IDP by region and ALDI score, in response to axial compression for mid-sagittal (top) and mid-coronal (bottom) paths. *: $p < 0.05$

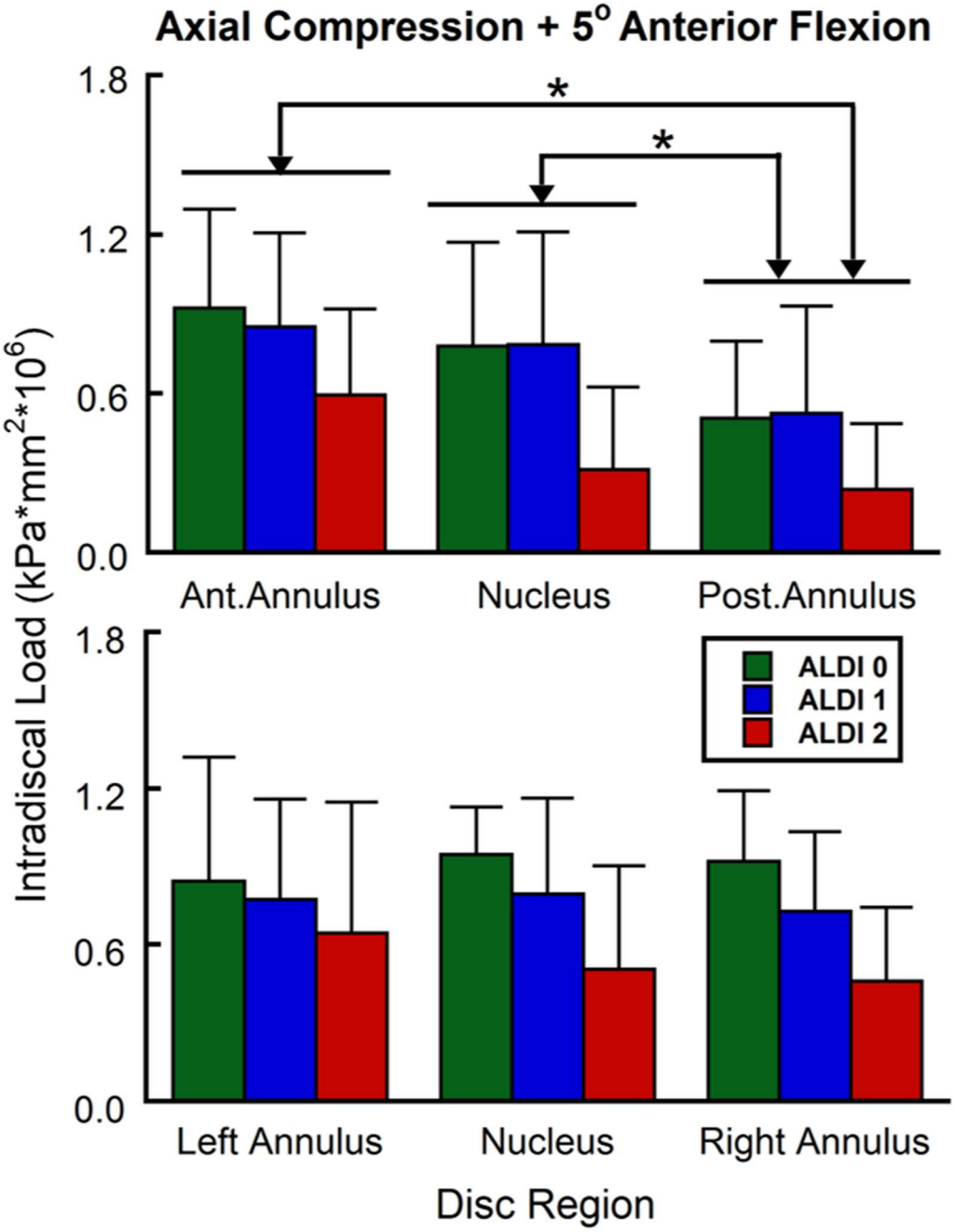

Figure 3.9 Mean IDP by region and ALDI score, in response to axial compression and combined anterior flexion for mid-sagittal (top) and mid-coronal (bottom) paths. *: $p < 0.05$

Spatial Heterogeneity

Under axial compressive loading, average deviation in IDP from the mean was lower in the NP as compared to all AF regions ($p<0.001$; Figure 3.10). Along the mid-coronal path, the average deviation was higher for ALDI score 0 vs. 1 ($p=0.013$) when all three regions were pooled.

Under axial compression with an applied 5 degrees of anterior flexion, the average deviation in IDP from the mean was higher in the anterior AF as compared to both the NP and posterior AF regions ($p<0.007$; Figure 3.11). Additionally, this average deviation was higher in the left and right AF regions as compared to the NP ($p\leq0.006$). Along the mid-sagittal path, the average deviation was higher in IVDs with an ALDI score of 0 as compared to those with an ALDI score of 2 ($p=0.038$) when all three regions were pooled.

Regional Maximum IDP and IDP Gradient

Under axial compressive loading, no differences in regional maximum IDP were found when comparing AF regions ($p\geq0.061$; Figure 3.12) No dependence of regional maximum IDP on ALDI score was found between these regions ($p>0.183$) No differences in IDP gradients were found when comparing all AF regions ($p>0.202$; Figure 3.13). No dependence of IDP gradient on ALDI score was found between these regions ($p>0.174$).

Under axial compression with an applied 5 degrees of anterior flexion, regional maximum IDP was higher in the anterior AF as compared to posterior AF ($p<0.0001$; Figure 3.14). Along the mid-sagittal path, regional maximum IDP was higher in IVDs

with an ALDI score of 0 as compared to those with an ALDI score of 2 (p=0.047). No differences in IDP gradients were found among all AF regions (p>0.293; Figure 3.15). No dependence of IDP gradient on ALDI score was found for any AF region (p>0.324).

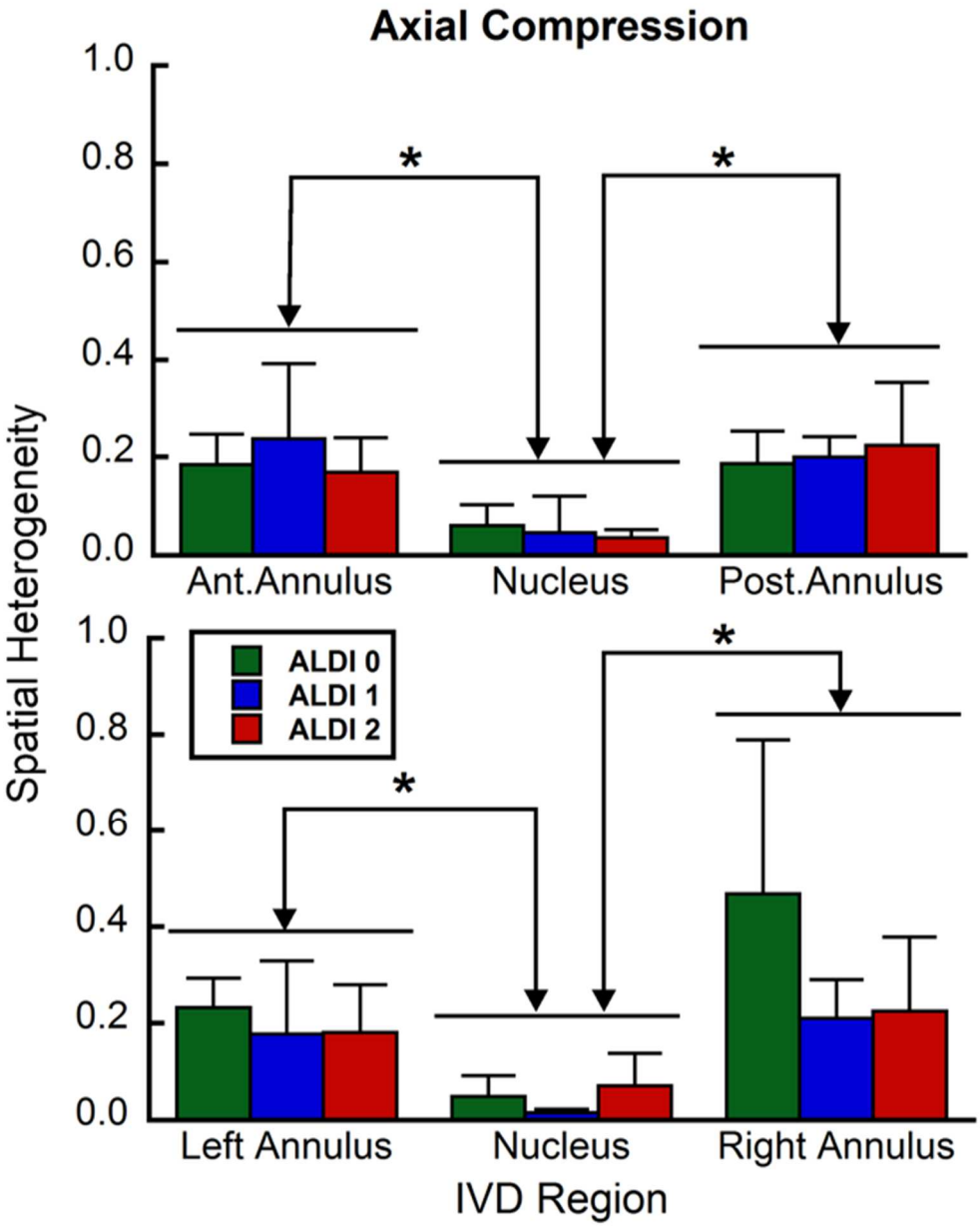

Figure 3.10 Spatial heterogeneity by region and ALDI score, in response to axial compression for mid-sagittal (top) and mid-coronal (bottom) paths. *: p <0.05

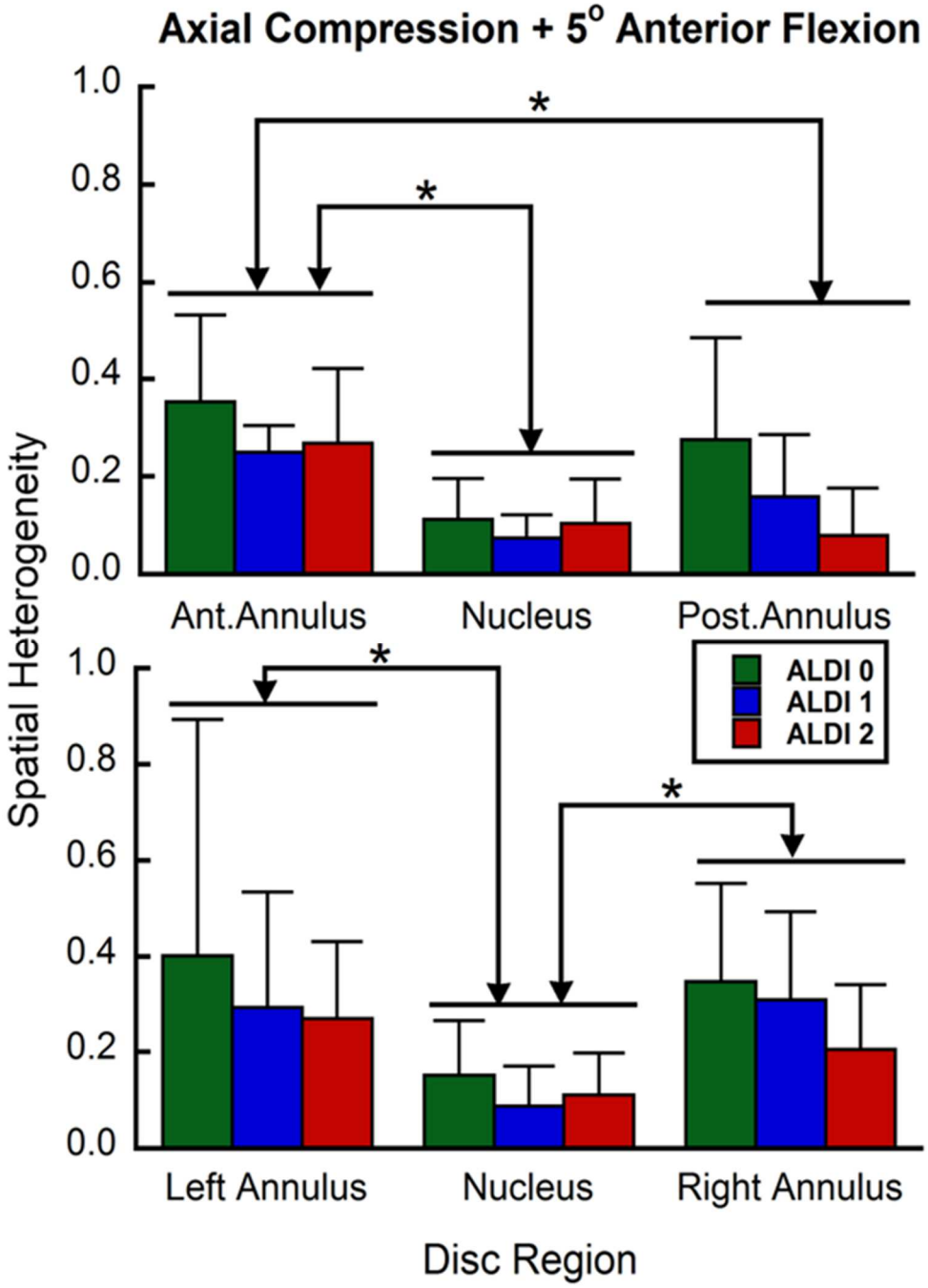

Figure 3.11 Spatial heterogeneity by region and ALDI score, in response to axial compression and combined anterior flexion for mid-sagittal (top) and mid-coronal (bottom) paths. *: $p < 0.05$

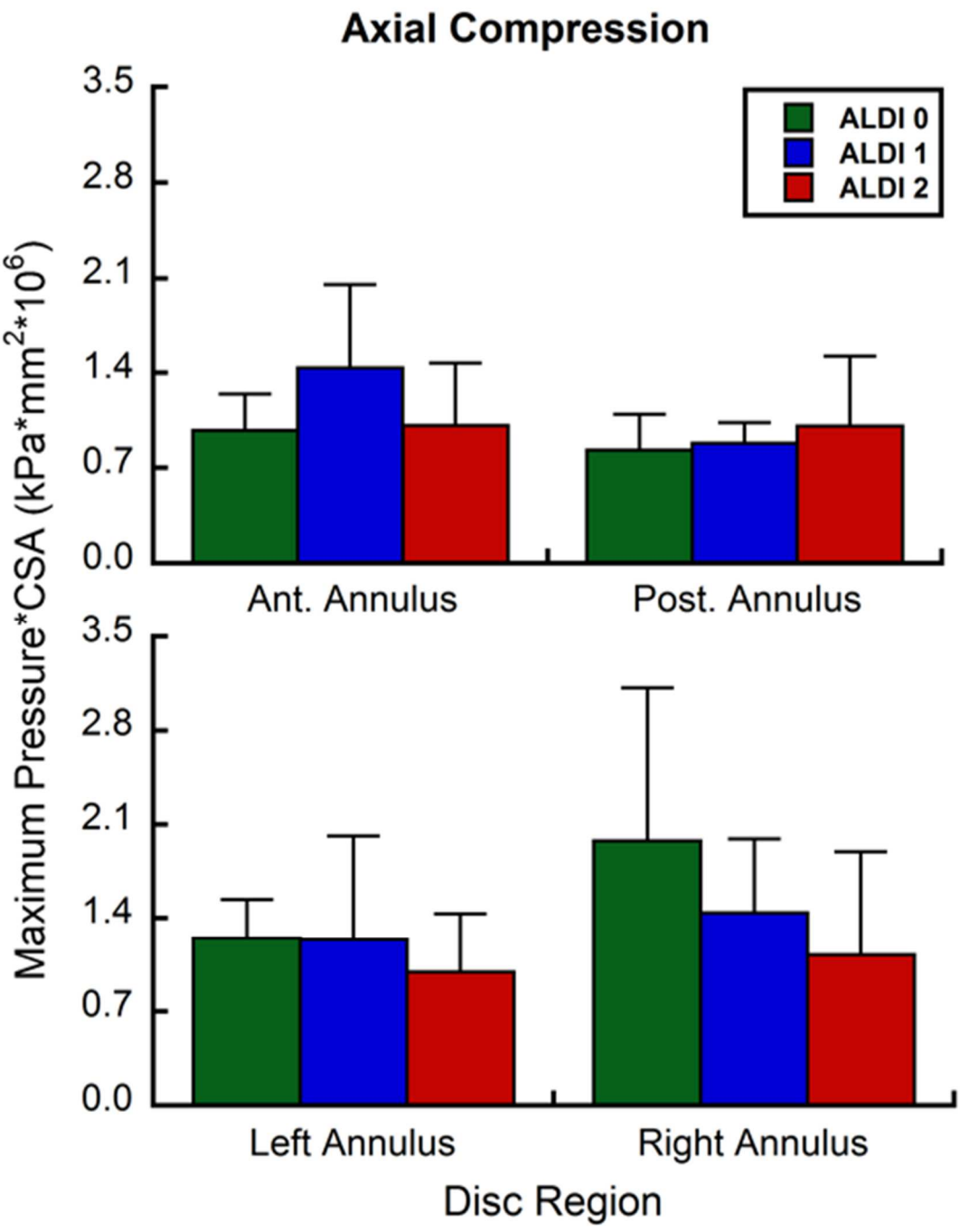

Figure 3.12 Maximum IDP by region and ALDI score, in response to axial compression for mid-sagittal (top) and mid-coronal (bottom) paths.

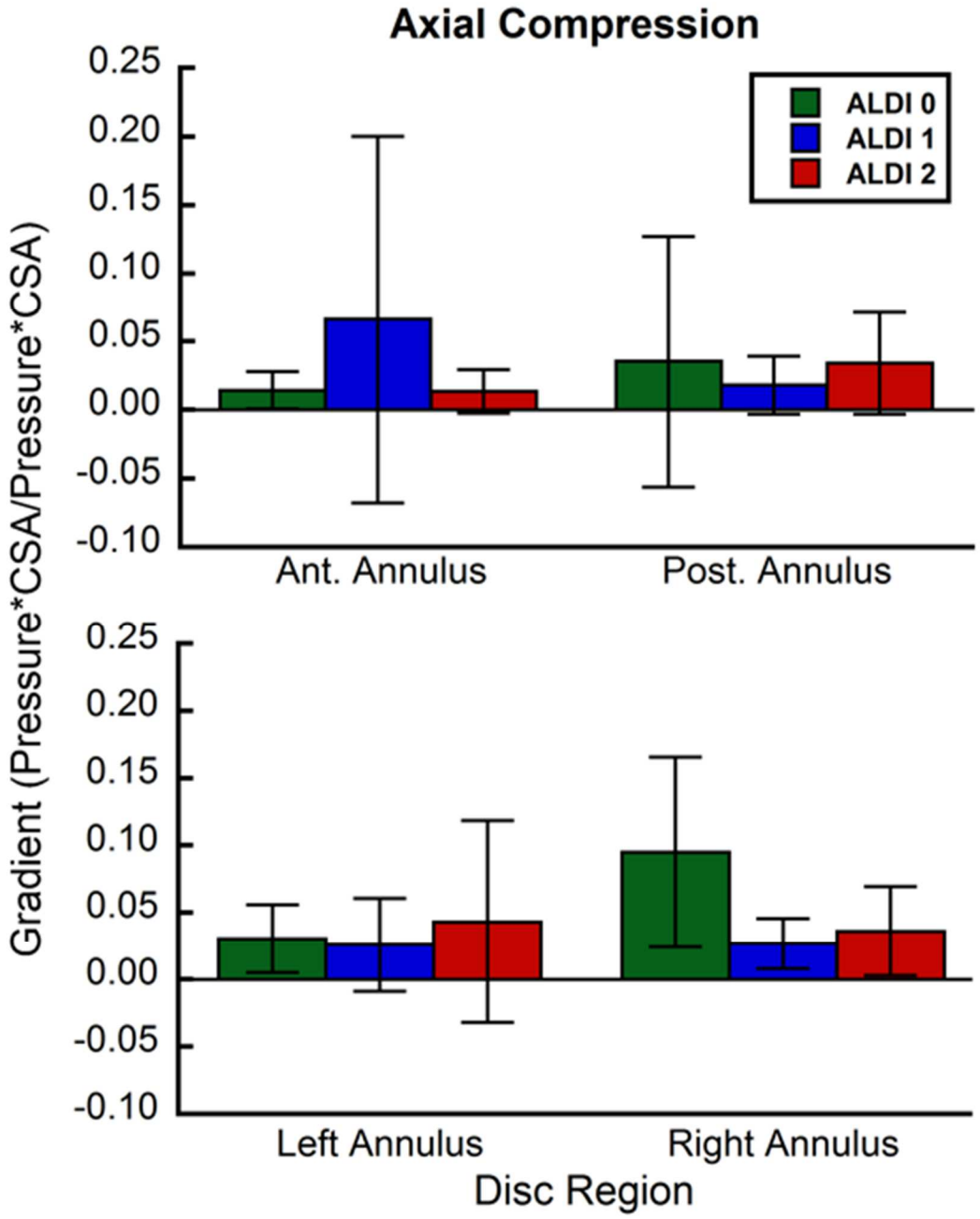

Figure 3.13 IDP gradient by region and ALDI score, in response to axial compression for mid-sagittal (top) and mid-coronal (bottom) paths.

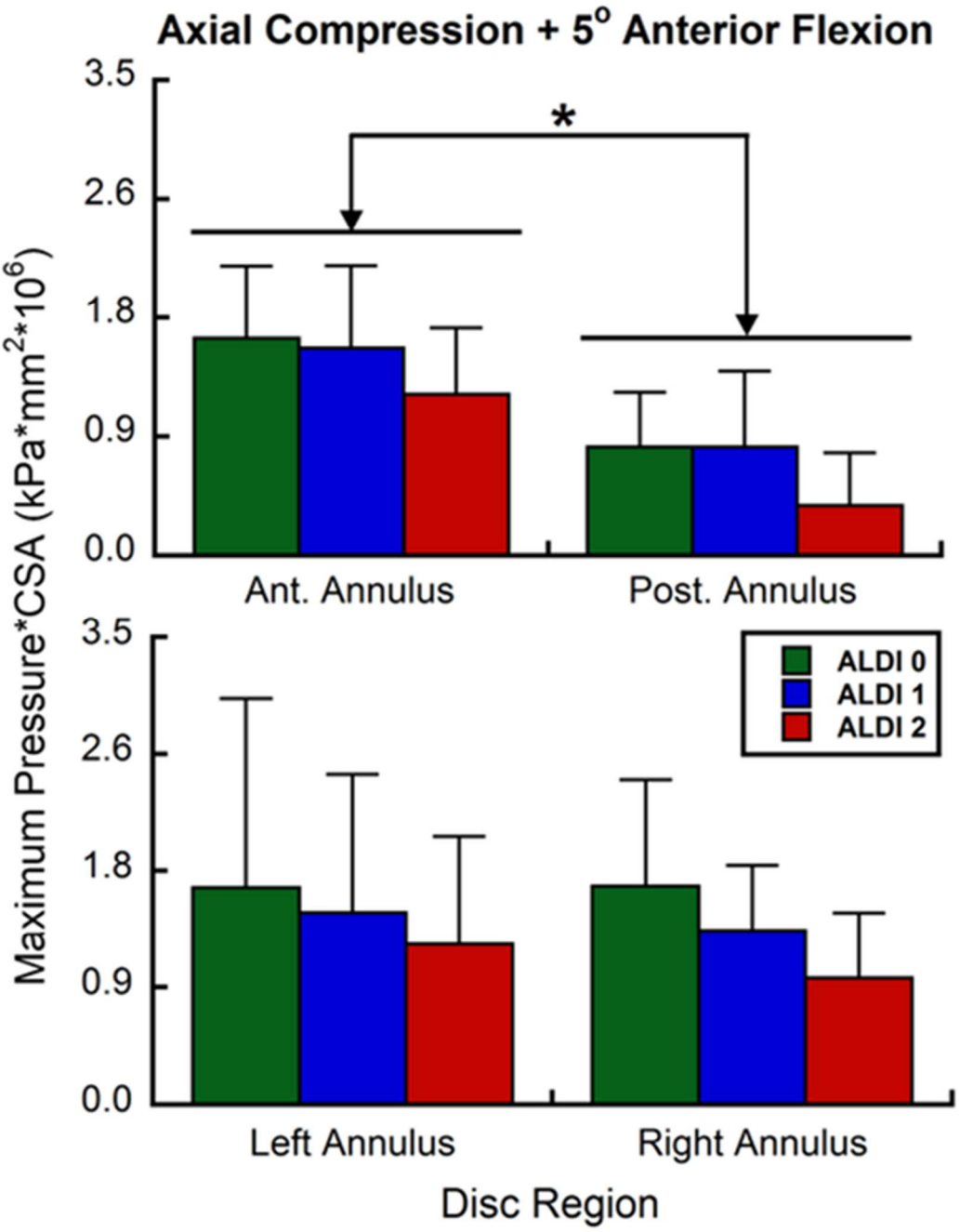

Figure 3.14 Maximum IDP by region and ALDI score, in response to axial compression and combined anterior flexion for mid-sagittal (top) and mid-coronal (bottom) paths *: $p<0.05$

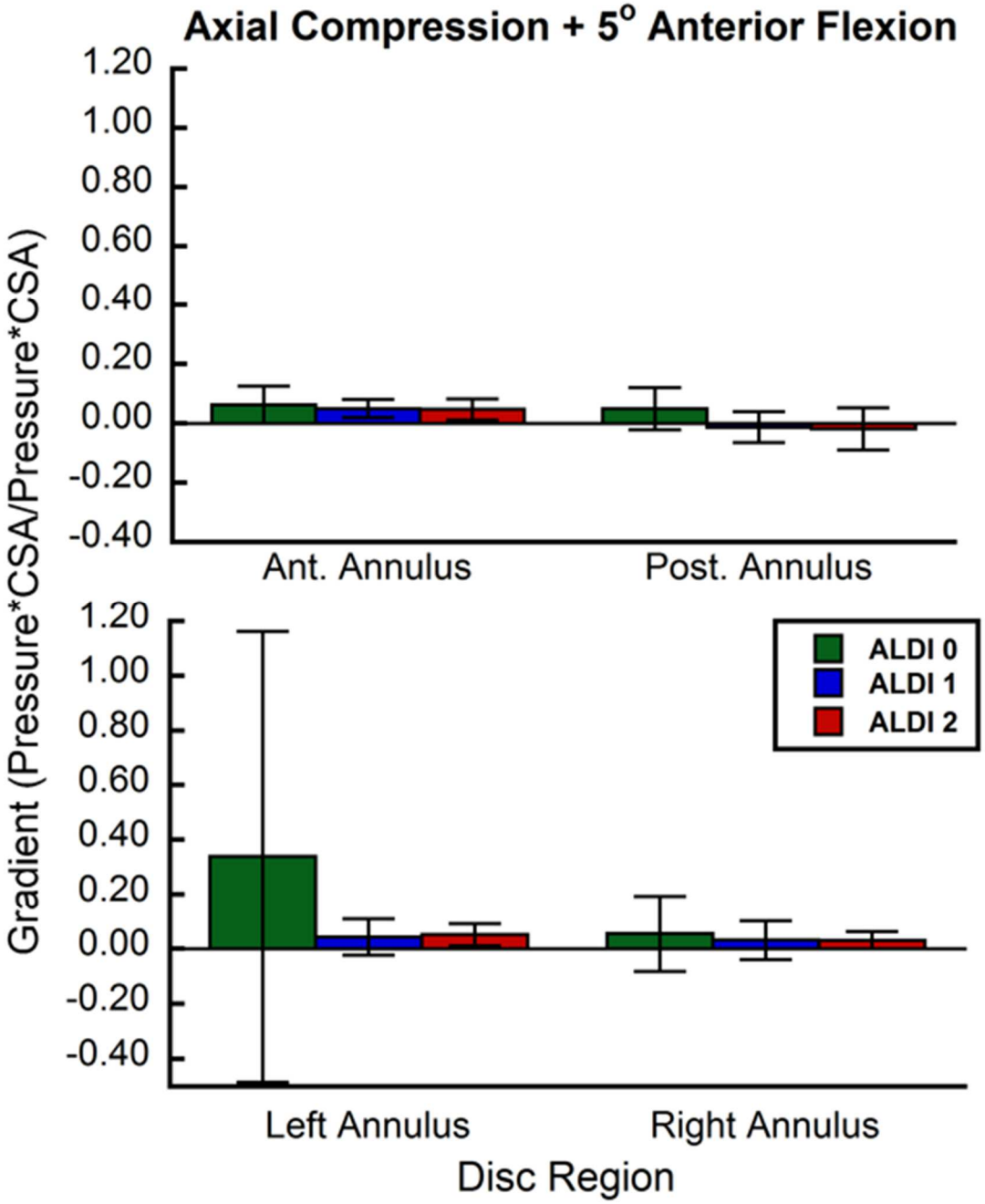

Figure 3.15 IDP gradient by region and ALDI score, in response to axial compression and combined anterior flexion for mid-sagittal (top) and mid-coronal (bottom) paths

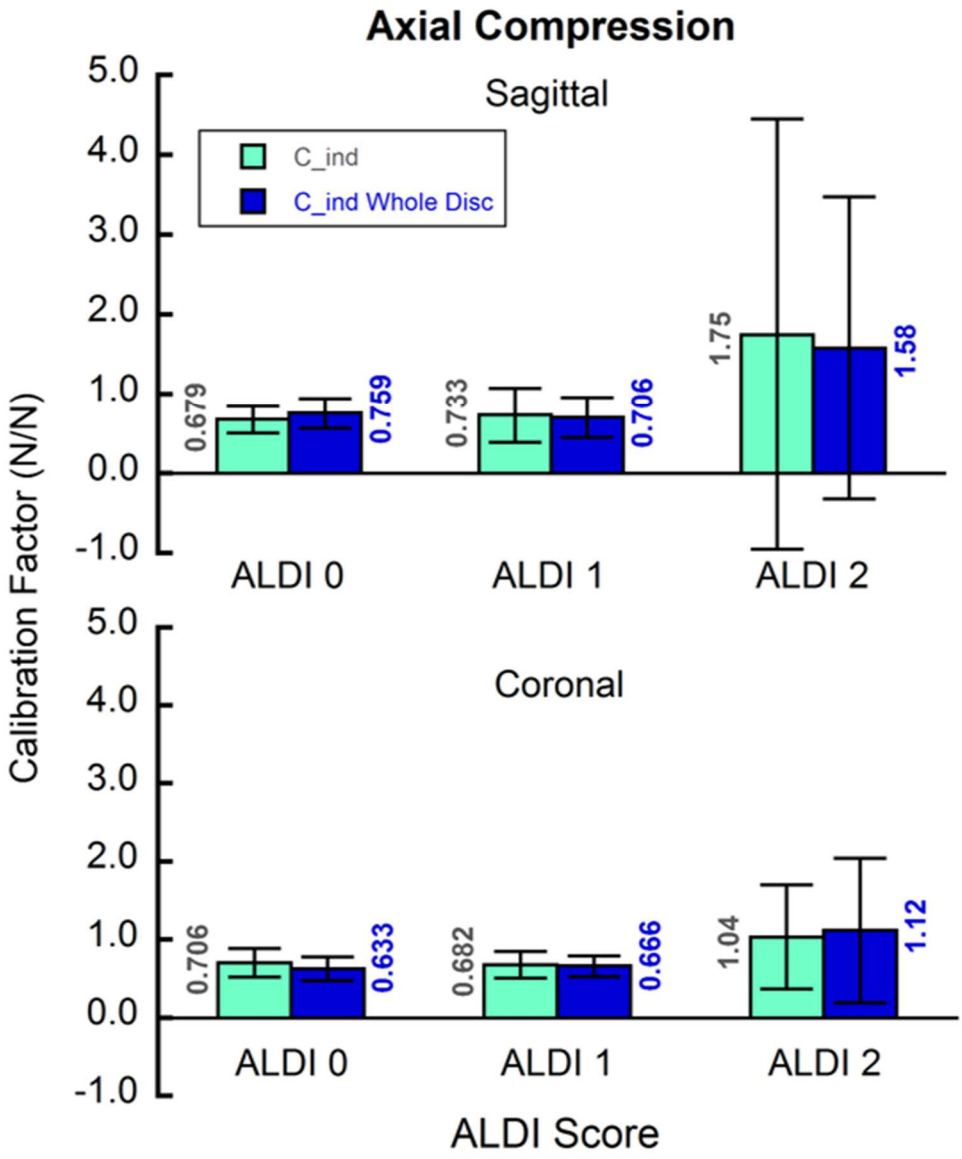

Figure 3.16 Average calibration factor values versus ALDI score, calculated for average IDP across the NP ('C_ind') and average IDP across the entire IVD ('C_ind Whole Disc'). Calibration values obtained under axial compression for mid-sagittal (top) and mid-coronal (bottom) paths.

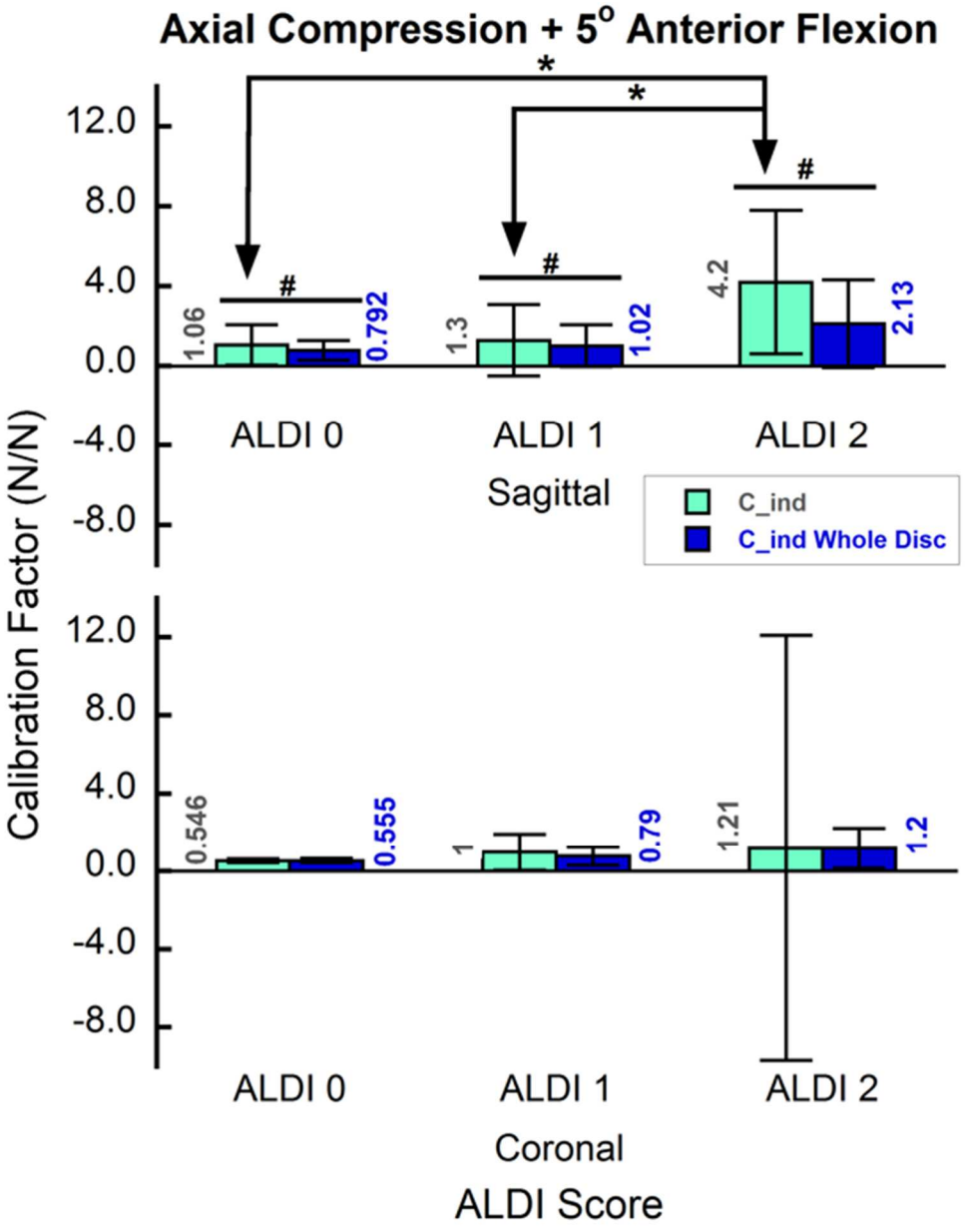

Figure 3.17 Average calibration factor values versus ALDI score, calculated for average IDP across the NP ('C_ind') and average IDP across the entire IVD ('C_ind Whole Disc'). Calibration values obtained under axial compression and combined anterior flexion for mid-sagittal (top) and mid-coronal (bottom) paths. *,#: $p<0.05$.

IVD Calibration Values

Under axial compressive loading, no dependence of NP-measured calibration factor on ALDI score was found across either mid-sagittal or mid-coronal path ($p>0.182$). No dependence of whole IVD-measured calibration factor on ALDI score was found across either mid-sagittal or mid-coronal path ($p>0.158$). Additionally, no differences in calibration factor when comparing NP-measured and whole IVD-measured calibration values across either mid-sagittal or mid-coronal paths ($p>0.707$; Figure 3.16).

Under axial compressive loading with an applied 5 degrees of anterior flexion, NP-measured calibration factor was higher in IVDs receiving ALDI scores of 2 as compared to those receiving both ALDI scores of 1 and 0, along the mid-sagittal path ($p=0.017$). No dependence of NP-measured calibration factor on ALDI score was found along the mid-coronal path ($p=0.138$). No dependence of whole IVD-measured calibration factor on ALDI score was found across either mid-sagittal or mid-coronal path ($p>0.131$). Along the mid-sagittal path, mean calibration factor was higher in whole IVD-measured calibration values as compared to NP-measured calibration values ($p=0.008$). No differences were found between these measurements along the mid-coronal path ($p=0.289$; Figure 3.17).

DISCUSSION

IVD degeneration is strongly associated with back pain, and results in an overall loss of IDP; however, it is not fully understood how degeneration affects the biomechanics of adjacent vertebrae. Therefore, investigation of the relationship between IDP and disc degeneration has implications in understanding the propagation or initiation

of vertebral fractures. In this study, the overall goal was to determine the extent of this correspondence by comparing IDP measurements with non-invasive, QCT-based assessments of disc health. As expected, anterior flexion induced both higher average loads and higher maximum loads within the anterior AF region of the IVD. The spatial load distribution was most homogenous within the NP, regardless of the type of applied load and disc score. This suggests that the NP region can maintain uniform IDP in different postures, and in the face of degeneration. IDP measurements in IVDs receiving an ALDI score of 2 tended to be lowest across all loading scenarios, and in all IVD regions except for the posterior AF under compressive loading. This is consistent with earlier findings by Pollintine et al., which notes that under severe disc degeneration, axial loads in the spinal column tend to shift from the IVD to the neural arch in both flexural and erect postures[38]. No differences in the spatial distribution of IDP were found between ALDI scores of 0 and 1. This may indicate that that the ALDI grading scale may not adequately reflect or discern functional changes for moderate levels of degeneration, or be able to discern early changes in levels of degeneration.

The primary strengths of this study are based primarily in its direct comparison of IDP to a non-invasive, QCT-based clinical assessment of IVD degeneration. Although MRI is generally preferred for spinal imaging, QCT is more practical in terms of speed, availability, cost, and patient needs (claustrophobia, existing metallic implants).[39,40] Therefore, developing and validating a grading scale that informs intradiscal mechanics as a result of disc degeneration could further inform studies of back pain and spinal mechanics. Furthermore, QCT-based finite element models are used in vertebral fracture

prediction analysis.[32,41] Thus, correlation of IDP with varying levels of IVD degeneration could improve boundary conditions of these models, and add to or improve the existing knowledge base of vertebral fracture analysis.

Additionally, the experimental setup of this study ensures both accuracy and speed in data collection. By utilizing spinal segments consisting of three vertebrae and the two IVDs –along with the use of an adjustable pressure transduce-actuator assembly—IDP measurements can be taken across both sagittal and coronal paths in quick succession. Spinal segments also left posterior elements intact to ensure physiologic loading conditions. This study was also one of few that measured IDP collected along mid-coronal paths.[42] By collecting IDP distribution along the coronal plane in IVDs loaded in axial compression and axial compression with applied anterior flexion, a better overall understanding of intradiscal mechanics can be developed.

Several limitations of this study will be addressed. First, the sample size for this study—twenty-six spinal segments, fifty-one IVDs—is relatively small, and must be considered when interpreting the results. One IVD was excluded from IDP measurement, as imaging revealed the presence of bridging osteophytes within the disc space that may have damaged the sensitive pressure transducer. The sample size is further limited by the decision to test IVDs of a given spinal segment in only one of each of the two loading conditions, instead of testing IVDs in both loading conditions. This decision was made as a result of the time constraint associated with testing IVDs in different loading scenarios. The amount of time required for testing both loading scenarios would result in discs becoming overly dehydrated, which may have affected the results of the study.

Second, the morphometric analysis utilized to determine the locations of intradiscal boundaries—the beginning and ends of the AF, and the two AF/NP boundaries—are subject to the visibility of QCT images. In the case of severely degenerated discs, the boundary between AF and NP can be difficult to discern. Thus, improper placement of points within the morphometric analysis as a result of this lack of clarity may affect the region of interest when determining regional IDP. However, to combat this issue, the NP region was approximated as the entirety of a centralized region within the IDP distribution that could vary up to 10%, as described in literature.[11] Four IVDs required the use of this approximation, all of which received an ALDI score of 2. Third, the method in which the IDP distribution is separated into its AF regions may influence measurements on spatial heterogeneity. The rise and fall of IDP seen at the ends of the AF regions (anterior, posterior, left, right) may add or detract from average spatial heterogeneity measurements collected these regions. After analysis had taken place, revisiting a past study revealed that pressure transducers tend to record little in the outermost 3mm of the AF.[43] In future studies, this adjustment should be noted and applied to IDP distributions, namely when regional analysis of the AF region is of interest. Finally, the ALDI scores assigned to the IVDs in question were administered by one grader, and the scoring system itself it not validated with inter- or intra-observer reliability.

This study extends prior investigations on the effect of disc degeneration on intradiscal pressure distribution. Measurements of stress distributions within IVDs by Adams et al. revealed homogeneity of the NP region, and large spikes in the AF regions

of the disc as a result of degeneration[11,12], which was confirmed throughout measurements of regional IDP measurements and spatial heterogeneity. Past studies of intradiscal pressure within point locations of lumbar porcine IVDs, showed that asymmetrical loading resulted in peak stresses in the AF region.[13] This was reciprocated in the data above, as samples loaded under anterior flexion tended showed greater average load and maximum loads in the anterior AF, when measured along the mid-sagittal path (Figures 3.9, 3.14).

Stefanakis et al., have recently investigated maximum stresses and stress gradients of the annulus regions.[20] This previous work showed that maximum stresses in the annulus regions tended to decrease with increasing grades of disc degeneration, in agreement with maximum load calculations shown in Figure 3.14. Additionally, this previous work also showed that large stress gradients are seen in the anterior AF under flexural loading conditions, and in the posterior AF under compressive loads. In this study, direct comparisons were not made between gradient calculations of different loading scenarios; however, a similar trend can be seen, when comparing Figures 3.13 and 3.15.

The development and calculation of IVD calibration values, for the validation of FE models was carried out by Dreischarf et al.[37] This previous work utilized intradiscal pressure measure measurements obtained from a central point within the NP, and FE-obtained IVD calibration values of 0.66±0.11 in healthy discs in erect posture. In this study, the compressive force and IDP obtained from the entirety of the NP were utilized to calculate IVD calibration values. In agreement to the previous study, average

calibration values for healthy IVDs under compression were similar to those of the experimentally obtained calibrations values (0.68±0.17; Figure 3.16). Additionally, this study was able to obtain average calibration values for IVDs of varying levels of degeneration. With increasing levels of disc degeneration, the IVD calibration values tended to increase in both compressive and flexural loading along the sagittal path. This signals a decrease in pressure across the NP, shifting posteriorly to the neural arch in flexural and erect postures, which also is consistent with previous findings.[3,19,38] Further development of individual calibration factors for IVDs of varying levels of degeneration will inform more robust FE-models, and improve the measurement of forces acting throughout the spine.

The outcomes of this research contribute to the body of knowledge existing within the field of biomechanics, specifically the relationships between IDP and disc degeneration. This study aimed to determine the level of correlation between a qualitative measure of IDP and a quantitative, non-invasive assessment of disc degeneration. In doing so, a test of the efficacy of the QCT-based ALDI grading scale for disc degeneration was carried out. Future work in improving the accuracy of these non-invasive methodologies may help in diagnosis and treatment for disc degeneration as well as in identifying how disc degeneration, by changing how load is transferred to the adjacent vertebra, can alter an individual's risk of vertebral fracture.

BIBLIOGRAPHY

1. O'Neill TW, Felsenberg D, Varlow J, Cooper C, Kanis JA, Silman AJ. *The Prevalence of Vertebral Deformity in European Men and Women: The European Vertebral Osteoporosis Study.* Vol 11. 1996. doi:10.1002/jbmr.5650110719.

2. Johnell O, Kanis JA, Odén A, et al. Mortality after osteoporotic fractures. *Osteoporosis International*. 2004;15(1):38–42. doi:10.1007/s00198-003-1490-4.

3. Adams MA, Pollintine P, Tobias JH, Wakley GK, Dolan P. Intervertebral disc degeneration can predispose to anterior vertebral fractures in the thoracolumbar spine. *Journal of Bone and Mineral Research*. 2006;21(9):1409–1416. doi:10.1359/jbmr.060609.

4. Sornay-Rendu E, Allard C, Munoz F, Duboeuf F, Delmas PD. Disc space narrowing as a new risk factor for vertebral fracture: The OFELY Study. *Arthritis and Rheumatism*. 2006;54(4):1262–1269. doi:10.1002/art.21737.

5. Sornay-Rendu E, Munoz F, Duboeuf F, Delmas PD. Disc space narrowing is associated with an increased vertebral fracture risk in postmenopausal women: the OFELY Study. *Journal of Bone and Mineral Research.* 2004;19(12):1994–1999. doi:10.1359/JBMR.040904.

6. Arden NK, Griffiths GO, Hart DJ, Doyle D V, Spector TD. The association between osteoarthritis and osteoporotic fracture: the Chingford Study. *British Journal of Rheumatology*. 1996;35(12):1299–1304.

7. Urban JP, McMullin JF. Swelling pressure of the lumbar intervertebral discs: influence of age, spinal level, composition, and degeneration. *Spine*. 1988;13(2): 179–187.

8. Michalek AJ, Iatridis JC. Penetrating annulus fibrosus injuries affect dynamic compressive behaviors of the intervertebral disc via altered fluid flow: An analytical interpretation. *Journal of Biomechanical Engineering*. 2011; 133(8):084502. doi:10.1115/1.4004915.

9. Miller JA, Schmatz C, Schultz AB. Lumbar disc degeneration: correlation with age, sex, and spine level in 600 autopsy specimens. *Spine*. 1988;13(2):173–178. doi:10.1097/00007632-198802000-00008.

10. De Schepper EIT, Damen J, van Meurs JBJ, et al. The association between lumbar disc degeneration and low back pain: the influence of age, gender, and individual radiographic features. *Spine*. 2010;35(5):531–536. doi:10.1097/BRS.0b013e3181aa5b33.

11. Adams MA, McNally DS, Dolan P. “Stress” distributions inside intervertebral discs. The effects of age and degeneration. *Journal of Bone and Joint Surgery. British Volume*. 1996;78(6):965–972.

12. McNally D, Adams M. Internal intervertebral disc mechanics as revealed by stress profilometry. *Spine*. 1992;17:66–73.

13. Ryan G, Pandit A, Apatsidis D. Stress distribution in the intervertebral disc correlates with strength distribution in subdiscal trabecular bone in the porcine lumbar spine. *Clinical Biomechanics*. 2008;23(7):859–869. doi:10.1016/j.clinbiomech.2008.03.066.

14. Dolan P, Luo J, Pollintine P, Landham PR, Stefanakis M, Adams M. Intervertebral disc decompression following endplate damage: implications for disc degeneration depend on spinal level and age. *Spine*. 2013;38(17):1473–1481. doi:10.1097/BRS.0b013e318290f3cc.

15. Edwards WT, Ordway NR, Zheng Y, McCullen G, Han Z, Yuan HA. Peak stresses observed in the posterior lateral anulus. *Spine*. 2001;26(16):1753–1759. doi:10.1097/00007632-200108150-00005.

16. Jalava T, Sarna S, Pylkkänen L, et al. Association between vertebral fracture and increased mortality in osteoporotic patients. *Journal of Bone and Mineral Research*. 2003;18(7):1254–1260. doi:10.1359/jbmr.2003.18.7.1254.

17. Homminga J, Weinans H, Gowin W, Felsenberg D, Huiskes R. Osteoporosis changes the amount of vertebral trabecular bone at risk of fracture but not the vertebral load distribution. *Spine*. 2001;26(14):1555–1561. doi:10.1097/00007632-200107150-00010.

18. Polikeit A, Nolte LP, Ferguson SJ. Simulated influence of osteoporosis and disc degeneration on the load transfer in a lumbar functional spinal unit. *Journal of Biomechanics*. 2004;37(7):1061–1069. doi:10.1016/j.jbiomech.2003.11.018.

19. Pollintine P, Dolan P, Tobias JH, Adams M. Intervertebral disc degeneration can lead to “stress-shielding” of the anterior vertebral body: a cause of osteoporotic vertebral fracture? *Spine*. 2004;29(7):774–782. doi:00007632-200404010-00012 [pii].

20. Stefanakis M, Luo J, Pollintine P, Dolan P, Adams M. Mechanical influences in progressive intervertebral disc degeneration. *Spine*. 2014;39(17):1365–1372. doi:10.1097/BRS.0000000000000389.

21. Hussein AI, Jackman TM, Morgan SR, Barest GD, Morgan EF. The intravertebral distribution of bone density: Correspondence to intervertebral disc health and implications for vertebral strength. *Osteoporosis International*. 2013;24(12):3021–3030. doi:10.1007/s00198-013-2417-3.

22. Mathis JM. Spine anatomy. In: *Percutaneous Vertebroplasty and Kyphoplasty*. New York: Springer. 2006:8–32. doi:10.1007/0-387-36083-2_2.

23. Urban JPG, Roberts S. Degeneration of the intervertebral disc. *Arthritis Research & Therapy*. 2003;5(3):120–130. doi:10.1186/ar629.

24. Urban JP, McMullin JF. Swelling pressure of the inervertebral disc: influence of proteoglycan and collagen contents. *Biorheology*. 1985;22(2):145–157.

25. Inoue N, Espinoza Orías AA. Biomechanics of Intervertebral Disk Degeneration. *Orthopedic Clinics of North America*. 2011;42(4):487–499. doi:10.1016/j.ocl.2011.07.001.

26. Bibby SRS, Jones DA, Lee RB, Yu J, Urban JPG. The pathophysiology of the intervertebral disc. In: *Joint, Bone, Spine*. 2001;68:537–542. doi:10.1016/S1297-319X(01)00332-3.

27. Smith LJ, Nerurkar NL, Choi K-S, Harfe BD, Elliott DM. Degeneration and regeneration of the intervertebral disc: lessons from development. *Disease Models & Mechanisms*. 2011;4(1):31–41. doi:10.1242/dmm.006403.

28. Roughley PJ, Melching LI, Heathfield TF, Pearce RH, Mort JS. The structure and degradation of aggrecan in human intervertebral disc. In: *European Spine Journal*. 2006;15(suppl. 3):326–332. doi:10.1007/s00586-006-0127-7.

29. Boos N, Weissbach S, Rohrbach H, Weiler C, Spratt KF, Nerlich AG. Classification of age-related changes in lumbar intervertebral discs: 2002 Volvo Award in basic science. *Spine*. 2002;27(23):2631–2644. doi:10.1097/01.BRS.0000035304.27153.5B.

30. Nachemson A. Lumbar intradiscal pressure. Experimental studies on post-mortem material. *Acta Orthopaedica Scandinavica. Supplementum*. 1960;31(43):1–103.

31. Thompson JP, Pearce RH, Schechter MT, Adams ME, Tsang IK, Bishop PB. Preliminary evaluation of a scheme for grading the gross morphology of the human intervertebral disc. *Spine*. 1990;15(5):411–415. doi:10.1097/00007632-199005000-00012.

32. Lane NE, Nevitt MC, Genant HK, Hochberg MC. Reliability of new indices of radiographic osteoarthritis of the hand and hip and lumbar disc degeneration. *Journal of Rheumatology*. 1993;20(11):1911–1918.

33. Pfirrmann CW, Metzdorf A, Zanetti M, Hodler J, Boos N. Magnetic resonance classification of lumbar intervertebral disc degeneration. *Spine*. 2001;26(17):1873–1878. doi:10.1097/00007632-200109010-00011.

34. Majumdar S, Link TM, Steinbach LS, Hu S, Kurhanewicz J. Diagnostic Tools and Imaging Methods in Intervertebral Disk Degeneration. *Orthopedic Clinics of North America*. 2011;42(4):501–511. doi:10.1016/j.ocl.2011.07.007.

35. Pearce R, Thompson J, Bebault G, Flak B. Magnetic resonance imaging reflects the chemical changes of aging degeneration in the human intervertebral disk. *Journal of Rheumatology. Supplement*. 1991;27:42–43.

36. Southern EP, Fye MA, Panjabi MM, Patel TC, Cholewicki J. Disc degeneration: a human cadaveric study correlating magnetic resonance imaging and quantitative discomanometry. *Spine*. 2000;25(17):2171–2175. doi:10.1097/00007632-200009010-00005.

37. Dreischarf M, Rohlmann A, Zhu R, Schmidt H, Zander T. Is it possible to estimate the compressive force in the lumbar spine from intradiscal pressure measurements? A finite element evaluation. *Medical Engineering & Physics.* 2013;35(9):1385–1390. doi:10.1016/j.medengphy.2013.03.007.

38. Pollintine P, Przybyla AS, Dolan P, Adams MA. Neural arch load-bearing in old and degenerated spines. *Journal of Biomechanics*. 2004;37(2):197–204. doi:10.1016/S0021-9290(03)00308-7.

39. Wood JC, Mo A, Gera A, Koh M, Coates T, Gilsanz V. Quantitative computed tomography assessment of transfusional iron overload. *British Journal of Haematology*. 2011;153(6):780–785. doi:10.1111/j.1365-2141.2011.08590.x.

40. Tins B. Technical aspects of CT imaging of the spine. *Insights into Imaging*. 2010;1(5–6):349–359. doi:10.1007/s13244-010-0047-2.

41. Genant HK, Wu CY, van Kuijk C, Nevitt MC. Vertebral fracture assessment using a semiquantitative technique. *Journal of Bone and Mineral Research*. 1993;8(9):1137–1148. doi:10.1002/jbmr.5650080915.

42. Buttermann GR, Beaubien BP. In vitro disc pressure profiles below scoliosis fusion constructs. *Spine*. 2008;33(20):2134–2142. doi:10.1097/BRS.0b013e31817d1d7f.

43. Dolan P, Adams MA. Recent advances in lumbar spinal mechanics and their significance for modelling. *Clinical Biomechanics*. 2001;16 Suppl 1:S8–S16. doi:10.1016/S0268-0033(00)00096-6.

VITA